Title

Shortening heparan sulfate chains prolongs survival and reduces parenchymal plaques in prion disease caused by mobile, ADAM10-cleaved prions

Journal

Acta Neuropathologica, 139(3)

ISSN

0001-6322

Authors

Aguilar-Calvo, Patricia
Sevillano, Alejandro M
Bapat, Jaidev
et al.

Publication Date

2020-03-01

DOI

10.1007/s00401-019-02085-x

Peer reviewed

HHS Public Access

Author manuscript

Acta Neuropathol. Author manuscript; available in PMC 2021 March 01.

Published in final edited form as:

Acta Neuropathol. 2020 March ; 139(3): 527–546. doi:10.1007/s00401-019-02085-x.

Shortening heparan sulfate chains prolongs survival and reduces parenchymal plaques in prion disease caused by mobile, ADAM10-cleaved prions

Patricia Aguilar-Calvo[1], **Alejandro M. Sevillano**[1], **Jaidev Bapat**[1], **Katrin Soldau**[1], **Daniel R. Sandoval**[2], **Hermann C. Altmeppen**[3], **Luise Linsenmeier**[3], **Donald P. Pizzo**[1], **Michael Geschwind**[4], **Henry Sanchez**[4], **Brian Appleby**[5,6], **Mark Cohen**[5,6], **Jiri G. Safar**[5,6], **Steven D. Edland**[7,8], **Markus Glatzel**[3], **K. Peter R. Nilsson**[9], **Jeffrey D. Esko**[2], **Christina J. Sigurdson**[1,10,11,#]

[1]Department of Pathology, University of California, San Diego (UCSD), La Jolla, CA, USA

[2]Department of Cellular and Molecular Medicine, University of California, San Diego (UCSD), La Jolla, CA, USA

[3]Institute of Neuropathology, University Medical Center Hamburg-Eppendorf (UKE), Hamburg, Germany

[4]Department of Neurology, Memory and Aging Center, University of California, San Francisco (UCSF), San Francisco, CA, USA

[5]Departments of Pathology and Neurology, Case Western Reserve University, Cleveland, OH, USA

[6]National Prion Disease Pathology Surveillance Center, Case Western Reserve University, Cleveland, OH, USA

[7]Department of Family Medicine & Public Health, University of California, San Diego (UCSD), La Jolla, CA USA

[8]Department of Neurosciences, University of California, San Diego (UCSD), La Jolla, CA USA

[9]Department of Physics, Chemistry, and Biology, Linköping University, Linköping, Sweden

[10]Department of Medicine, University of California, San Diego (UCSD), La Jolla, CA, USA

[11]Department of Pathology, Immunology, and Microbiology, University of California, Davis (UCD), Davis, CA, USA

[#]Corresponding author: Dr. Christina J. Sigurdson, Department of Pathology, UC San Diego, 9500 Gilman Dr., La Jolla, CA 92093, USA, Phone: +1 (858) 534 0978, csigurdson@ucsd.edu, fax: +1 (858) 246-0523.

Author contributions

PAC, KPRN, CJS, DRS, JDE designed experiments, PAC, AMS, JB, KS, DPP, KPRN performed the experiments, PAC, JB, LL, HCA, MG, SDE, MG, HS, JGS, KPRN, JDE, CJS, MC, BA analyzed experiments, and PAC and CJS wrote the manuscript.

The authors have declared that no conflict of interest exists.

Abstract

Cofactors are essential for driving recombinant prion protein into pathogenic conformers. Polyanions promote prion aggregation *in vitro*, yet the cofactors that modulate prion assembly *in vivo* remain largely unknown. Here we report that the endogenous glycosaminoglycan, heparan sulfate (HS), impacts prion propagation kinetics and deposition sites in the brain. Exostosin-1 haploinsufficient ($Ext^{+/-}$) mice, which produce short HS chains, show a prolonged survival and a redistribution of plaques from the parenchyma to vessels when infected with fibrillar prions, and a modest delay when infected with subfibrillar prions. Notably, the fibrillar, plaque-forming prions were composed of ADAM10-cleaved prion protein lacking a glycosylphosphatidylinositol-anchor, indicating these prions were mobile and assembled extracellularly. By analyzing the prion-bound HS using liquid chromatography mass spectrometry (LC-MS), we identified the disaccharide signature of HS differentially bound to fibrillar compared to subfibrillar prions, and found approximately 20-fold more HS bound to the fibrils. Finally, LC-MS of prion-bound HS from human patients with familial and sporadic prion disease also showed distinct HS signatures and higher HS levels associated with fibrillar prions. This study provides the first *in vivo* evidence of an endogenous cofactor that accelerates prion disease progression and enhances parenchymal deposition of ADAM10-cleaved, mobile prions.

Keywords

amyloid; neurodegeneration; glycosaminoglycans; ADAM10 cleavage

INTRODUCTION

More than 35 proteins aggregate into pathogenic fibrils in systemic and neurodegenerative disorders, including diabetes and Alzheimer's disease [22]. Fibril assembly is accelerated *in vitro* by diverse anionic polymers, such as RNA, heparin, and heparan sulfate (HS) [14, 16, 23], raising the question of whether endogenous polymers affect disease progression *in vivo*. Glycosaminoglycans (GAGs) are long polysaccharide chains containing repeating disaccharide units assembled on extracellular and membrane bound proteins. HS, a type of GAG, is structurally similar to the anticoagulant heparin and has been found associated with nearly all amyloids [5, 61, 66, 69, 97, 98, 100]. The specificity of HS - protein binding is profoundly affected by HS chain length as well as by the density and pattern of sulfation [62, 105, 114], which varies among cell types [93].

Prion diseases are rapidly progressive neurodegenerative disorders [86] caused by the misfolding of the cell surface expressed prion protein monomer, PrP^{C}, into a β-sheet-rich multimer, PrP^{Sc} [18, 20, 76, 87]. PrP^{Sc} can be arranged as distinct conformers, or strains, having different biochemical properties, cellular targets, and varying abilities to spread into the central nervous system (CNS) [8-10, 13]. For example, fibrillar prions spread poorly from extraneural entry sites into the CNS, whereas subfibrillar prions, which do not form plaques or ultrastructurally visible fibrils *in situ,* spread efficiently into the CNS [10-12, 52]. Yet the molecular mechanisms that govern prion assembly into fibrils or subfibrils and that determine how structure is linked to the capacity to spread are unknown.

Similar to other amyloidogenic proteins, prions bind GAGs, and *in vitro* studies have revealed that GAGs promote prion conversion and fibril assembly [6, 46, 113], enhance prion uptake [40-42], and stabilize PrP^C [109]. Shortening or de-sulfating HS chains abrogated the acceleration in fibril assembly and enhanced uptake of prions [46], supporting a role for HS in prion conversion. Additionally, HS co-localizes with prion plaques in brain sections from patients and prion-infected mice [66, 96], which together with the *in vitro* findings, suggest HS may impact prion aggregation, cell targeting, and spread *in vivo*.

Paradoxically, GAG mimetics delay prion disease in animals [1, 26, 28, 29, 56, 57], potentially due to stabilization of PrP^C [109] or competition with endogenous GAGs [17, 19]. These encouraging initial reports led to the treatment of five variant Creutzfeldt-Jakob disease (vCJD) patients with intraventricular pentosan polysulfate; four of five patients showed an extended survival as compared to the mean for vCJD. While the results were promising, a treatment effect due to differences in patient care could not be excluded [68, 80, 107].

To determine how HS modifications impact prion spread through the brain, here we altered HS chain length and tested the impact on prion assembly and replication *in vivo*. Using $Ext1^{+/-}$ mice that express shorter HS chains due to a reduction in exostosin-1 (Ext1) [60], the co-polymerase that assembles the HS chains [72], we assessed the spread of three conformationally diverse prion strains. *Ext1* haploinsuffuciency did not alter the conformation of any prion strain. Instead we found evidence that HS binds ADAM-10 cleaved, fibrillar prions, facilitates parenchymal plaque formation, and accelerates disease, yet only minimally binds to GPI-anchored, subfibrillar prions. Using mass spectrometry and immunohistochemistry, we found high levels of HS bound to fibrillar prions in mouse and human brain, and localized HS to the plaque core. Collectively, our results elucidate how HS impacts parenchymal prion plaque distribution in a strain specific manner, and indicate a rationale for selectively targeting the plaque-forming prions for treatment trials designed to disrupt the HS-prion interface.

METHODS

Prion transmission experiments in transgenic mice

$Ext1^{+/-}$ mice [60] were bred to wild type mice (C57BL/6) or *tg*a20 mice, which overexpress mouse PrP^C [31]. Mice were maintained under specific pathogen-free conditions on a 12:12 light/dark cycle. Groups of 5-16 male and female $Ext1^{+/-}$ and $Ext1^{+/+}$ littermate control mice (6-8 weeks old) were anesthetized with ketamine and xylazine and inoculated into the left parietal cortex with 30 μl of 1% prion-infected brain homogenate prepared from terminally ill mice.

Prion-inoculated mice were monitored three times weekly for the development of terminal prion disease, including ataxia, kyphosis, stiff tail, hind leg clasp, and hind leg paresis, and were then euthanized. The brain was halved, and one hemisphere was immediately fixed in formalin. Fixed brains were treated for 1 hour in 96% formic acid, post-fixed in formalin, cut into 2 mm transverse sections, and paraffin-embedded for histological analysis. A 2-3 mm transverse section was removed from the remaining hemisphere at the level of the

hippocampus/thalamus, embedded in optimal cutting temperature (OCT) compound and immediately frozen on dry ice. The remaining brain tissue was frozen for biochemical studies. Survival time was calculated from the day of inoculation to the day of terminal clinical disease.

Histopathology and immunohistochemical stains

Four micron sections were cut onto positively charged silanized glass slides and stained with hematoxylin and eosin (HE), or immunostained using antibodies for PrP [SAF84, epitope in the globular domain, amino acids 160–170 of mouse PrP (Cayman Chemical); 12F10, epitope in the globular domain, amino acids 144–152 of human PrP (Cayman Chemical); $sPrP^{G228}$, epitope in the proteolytically cleaved C-terminus, including amino acid 228G of mouse PrP (generated in the lab of co-author MG) [63])] as well as astrocytes (glial fibrillary acidic protein, GFAP), microglia (Iba1), and endothelial cells (CD31). For all mouse and most human PrP immunolabelling, sections were deparaffinized and incubated for 5 minutes in 96% formic acid, then washed in water for 5 minutes, treated with 5 μg/ml of proteinase-K (PK) for 7 minutes, and washed in water for 7 minutes. Sections were then placed in citrate buffer (pH 6), heated in a pressure cooker for 20 minutes, cooled for 5 minutes, and washed in distilled water. Sections were blocked and incubated with anti-PrP antibodies SAF84, $sPrP^{G228}$ (mouse brain sections), or 12F10 (human brain sections, sCJD and GSS-F198S cases) for 45 minutes followed by anti-mouse or anti-rabbit biotin (Jackson Immunolabs) for 30 minutes, and then streptavidin-HRP (Jackson Immunoresearch) for 45 minutes. Slides were then incubated with DAB reagent (Thermo Scientific) for 15 minutes and counterstained with hematoxylin. For the GSS-P102L case, brain sections were placed in 1.5 mM HCl in a microwave pressure cooker for 15 minutes, blocked and incubated with 3F4 (epitope in amino terminus of PrP, amino acids 109-112 of human PrP, [49]) for 1 hour, incubated with enzyme-conjugated polymer DAKO Envision for 30 minutes, and then DAKO DAB reagent for 1 minute prior to counterstaining with hematoxylin. The immunostaining was performed on a Lab Vision 480 Autostainer.

GFAP immunohistochemistry for astrocytes (1:6,000; DAKO) was performed on an automated tissue immunostainer (Ventana Discovery Ultra, Ventana Medical Systems, Inc) with a protease antigen retrieval (P2, Ventana) for 16 minutes.

For the PrP and CD31 (endothelial cells) dual immunolabelling, tissue sections were stained sequentially using anti-PrP SAF84 (1:250) and CD31 antibodies (1:150; Dianova) using the tyramide signal amplification system (TSA; ThermoFisher). Slides were stained on a Ventana Discovery Ultra (Ventana Medical Systems, Tucson, AZ, USA). Antigen retrieval was performed using a slightly basic treatment solution (CC1; pH 8.5, Ventana) for 92 minutes at 95 °C. Sections then were incubated in anti-PrP antibody for 32 minutes at 37 °C, followed by anti-mouse-HRP (UltraMap Detection Kit, Ventana) and TSA-Alexa 594. The antibodies were denatured by treatment in a citric acid-based solution, pH 6 (CC2, Ventana) for 24 minutes at 95 °C. Subsequently, the slides were incubated with anti-CD31 antibody (rat) for 32 minutes at 37 °C followed by rabbit anti-rat (1:500; Jackson ImmunoResearch) and detected using the OmniMap system (Ventana) to fluorescently label the CD31-expressing cells with TSA-Alexa 488.

For the PrP and HS dual immunolabelling, tissue sections were deparaffinized and epitopes were exposed by sequential treatment with formic acid, PK, and heated citrate buffer (pH 6) as described above for PrP staining. Sections were blocked and incubated with anti-PrP [SAF-84 (1:250) or 12F10 (1:400)] and anti-HS [10E4 (1:200; AMS Bioscience)] antibodies for 45 minutes followed by anti-mouse IgM biotin (1:500; Jackson Immunolabs) for 30 minutes and streptavidin-HRP (1:2,000; Jackson Immunoresearch) for 45 minutes, and then incubated with tyramide-Alexa488 (Invitrogen) for 10 minutes. Finally sections were incubated with anti-mouse IgG – CY3 (1:200; Jackson Immunolabs), nuclei were labeled with DAPI, and slides were mounted with fluorescent mounting medium (Dako). As controls for the HS stain, a subset of duplicate slides were treated with 8 milli-units of heparin lyases I, II, and III for one hour prior to immunostaining. Isotype immunoglobulin controls, single sections immunostained for PrP or HS, and prion negative cases were also included.

For quantitative analysis of microglial inflammation in *tg*a20$^{+/-}$*Ext1*$^{+/-}$ and *tg*a20$^{+/-}$*Ext1*$^{+/+}$ mice, brain regions containing cerebral cortex, hippocampus, thalamus, hypothalamus, and cerebellum were imaged (approximately 6 fields per mouse) using the Olympus EX41 microscope with DP Controller. Images were converted to grayscale and FIJI (an ImageJ based image processing software) was used to measure the total brain area and quantify microglia using the “Measure” function. Activated microglia were demarcated using the “Find the edges” function and particle analysis was used to measure the area occupied by microglia. The total area covered by microglia was divided by the total area in each brain region.

For the Alcian blue stain, brain sections were deparaffinized and incubated for 3 minutes in 3% acetic acid, then stained in Alcian blue solution in the microwave for 30 seconds, cooled for 40 minutes, washed in distilled water, and counterstained in nuclear fast red solution for 5 minutes. For the Congo red staining, slides were deparaffinized, fixed in 70% ethanol for 10 minutes, immersed in an alkaline solution and then stained with Congo red solution for 20 minutes.

Histopathologic lesion profiles

Brain lesions from *Ext1*$^{+/-}$ and *Ext1*$^{+/+}$ prion-infected mice were scored for the level of spongiosis, gliosis, and PrP immunological reactivity on a scale of 0–3 (0 = not detectable, 1 = mild, 2 = moderate, 3 = severe) in 9 regions including grey and white matter: (1) dorsal medulla, (2) cerebellum, (3) hypothalamus, (4) medial thalamus, (5) hippocampus, (6) septum, (7) medial cerebral cortex dorsal to hippocampus, (8) cerebral peduncle, and (9) cerebellar peduncle. A sum of the three scores resulted in the value obtained for the lesion profile for the individual animal and was depicted in the ‘radar plots’. Two investigators blinded to animal identification performed the histological analyses.

Western blot and glycoprofile analyses

PrP^{Sc} was concentrated from 10% brain homogenate in phosphate buffered saline (PBS) (w/v) by performing sodium phosphotungstic acid precipitation prior to western blotting [110]. Briefly, 20 μl of 10% brain homogenate in an equal volume of 4% sarkosyl in PBS

was digested with benzonase™ (Sigma) followed by treatment with 20 μg/ml PK at 37 °C for 30 minutes. After addition of 4% sodium phosphotungstic acid in 170 mM $MgCl_2$ and protease inhibitors (Complete TM, Roche), extracts were incubated at 37 °C for 30 minutes and centrifuged at 18,000 x *g* for 30 minutes at 25 °C. Pellets were resuspended in 2% sarkosyl prior to electrophoresis and immunoblotting. Samples were electrophoresed through a 10% NuPage Bis-Tris gel (ThermoFisher Scientific) and transferred to nitrocellulose by wet blotting. Membranes were incubated with monoclonal antibody POM19 [discontinuous epitope at C-terminal domain, amino acids 201–225 of the mouse PrP [85]] or polyclonal antibody $sPrP^{G228}$ followed by incubation with an HRP-conjugated IgG secondary antibody. The blots were developed using a chemiluminescent substrate (Supersignal West Dura ECL, ThermoFisher Scientific) and visualized on a Fuji LAS 4000 imager. Quantification of PrP^{Sc} glycoforms was performed using Multigauge V3 software (Fujifilm). For mCWD, 100 μl of 10% brain homogenate was digested with 100 μg/ml PK prior to electrophoresis through a 10% NuPage Bis-Tris gel.

For quantifying the level of PrP^{C} expression in uninfected mice and PrP^{Sc} in prion-infected mice, the total protein concentration was measured in brain homogenates by bicinchoninic acid assay (Pierce) and equivalent protein levels were immunoblotted as described. Membranes were also probed for actin (Genetex) (PrP^{C} analysis only).

Conformation stability assay

Prion strain stability in guanidine hydrochloride (GdnHCl) was measured as previously described [82]. In brief, 10% brain homogenates in PBS (w/v) were denatured for 1 hour in increasing concentrations of GdnHCl from 0 to 6M. Samples were then diluted in a Tris-based lysis buffer (10 mM Tris-HCl, 150 mM NaCl, 10 mM EDTA, 2% sarkosyl, pH 7.5) to 0.15 M GdnHCl and digested with PK at a ratio of 1:500 (1 μg PK : 500 μg total protein) for 1 hour at 37 °C. The digestion was stopped with 2 mM phenylmethylsulfonyl fluoride (PMSF) and protease inhibitors (Complete-TM, Roche) followed by centrifugation at 18,000 x *g* for 1 hour. The pellets were washed in 0.1 M $NaHCO_3$ (pH 9.8) and centrifuged at 18,000 x *g* for 20 minutes. The pellets were then denatured in 6 M guanidine isothiocyanate (GdnSCN), diluted with 0.1 M $NaHCO_3$, and coated passively onto an ELISA plate. PrP was detected with biotinylated-POM1 antibody (epitope in the globular domain, amino acids 121–231 of the mouse PrP [85]), a streptavidin HRP-conjugated secondary antibody, and a chemiluminescent substrate. The PrP stability was measured in a minimum of 3 independent experiments for each strain, always comparing $Ext1^{+/-}$ with $Ext1^{+/+}$ (3–4 mice per strain).

h-FTAA staining and fluorescence life time imaging (FLIM)

Sections (10 μm) of OCT-embedded brain samples were cut onto positively charged silanized glass slides, dried for 1 hour, and fixed in 100% then 70% ethanol for 10 minutes each. After washing with deionized water, sections were equilibrated in PBS, pH 7.4, for 10 minutes. Heptamer-formyl thiophene acetic acid (h-FTAA) was diluted in PBS to a final concentration of 1.5 μM and added to the sections. The sections were incubated with h-FTAA for 30 minutes at room temperature, washed with PBS, and mounted using Dako fluorescence mounting medium. The fluorescence decay of h-FTAA bound to PrP aggregates was collected using an inverted Zeiss (Axio Observer.Z1) LSM 780 microscope

(Carl Zeiss MicroImaging GmbH) equipped with a modular FLIM system from Becker and Hickl. In this setup, the emitted photons were routed through the direct coupling confocal port of the Zeiss LSM 780 scanning unit and detected by a Becker and Hickl HPM-100-40 hybrid detector. Data were recorded by a Becker and Hickl Simple-Tau 152 system (SPC-150 TCSPC FLIM module) with the instrument recording software SPCM version 9.42 in the FIFO image mode, 256 × 256 pixels, using 256 time channels (Becker and Hickl GmbH). For all acquisitions, a T80R20 main beam splitter was used and the pinhole was set to 20.2 μm. Scanning area was set to 235.7 μm × 235.7 μm, with a scanning resolution of 512 × 512 pixels. A Plan-Apochromat 40 × / 1.3 Oil DIC objective lens was used and a 510 nm longpass filter was positioned in front of the hybrid detector. Excitation utilized the 490 nm laser line from the pulsed tunable In Tune laser (Carl Zeiss MicroImaging GmbH) with a repetition rate of 40 MHz. Data was subsequently analyzed in SPCImage version 3.9.4 (Becker and Hickl GmbH), fitting each of the acquired decay curves to a tri-exponential function and color coded images, as well as distribution histograms, showing the intensity-weighted mean lifetimes generated with the same software. The procedure of staining and FLIM imaging protein aggregates with h-FTAA is described in detail in reference [71].

Human patients with sporadic or familial prion disease

Brain samples from patients with sporadic Creuzfeldt-Jakob disease (sCJD) or Gerstmann-Sträussler-Scheinker disease (GSS) were used to investigate how the level of HS molecules bound to PrP^{Sc} correlated with the histopathologic lesions. The sCJD brain samples originated from patients referred to the UC San Francisco (UCSF) Memory and Aging Center for rapidly progressive neurologic disease. All patients had extensive clinical testing, including brain MRI as well as CSF analysis for 14-3-3, neuron-specific enolase (NSE), and total tau. All were classified as probable sCJD by UCSF clinical and radiological diagnostic criteria [33, 102]. Genetic disease was excluded by *PRNP* (PrP gene) analysis. The mean age of sCJD patients at disease onset was 59 ± 5 years (mean ± SD) and the duration of clinical neurologic signs ranged from 1.5 to 24 months (10 ± 9 months).

The GSS brain samples were received and characterized at the National Prion Disease Pathology Surveillance Center (NPDPSC). The mean age of GSS-F198S patients at disease onset was 57 ± 8 years. The duration of clinical neurologic signs markedly varied from 63 to 120 months (86 ± 25 months). Of the familial prion disease cases, the GSS-P102L patient showed the earliest age of disease onset (22 years) and the shortest disease duration (23 months).

For all patients, the *PRNP* open reading frame was sequenced to define the genotype at polymorphic codon 129 (methionine or valine) and to test for mutations in the PrP sequence. Genomic DNA was extracted from frozen brain tissue samples using Qiagen QIAamp DNA minikit (Qiagen, Gaithersburg, MD) according to the manufacturer's protocol, and a 760-bp fragment corresponding to the human PrP gene (residues 5 to 258) was amplified by PCR using primers HRM-F (5'-TATGTGGACTGATGTCGGCCTCTGCAAGAAGCGC-3') and HRM-R (5'-CCACCTCAATTGAAAGGGCTGCAGGTGGATAC-3') with defined cycling conditions [39, 53]. The Met/Val polymorphism at codon 129 and mutation of the *PRNP* coding region were determined by deep (63) or direct Sanger sequencing as previously

described [53, 79]. Nucleotide sequences from both deep and Sanger sequencing were analyzed using DNAStar Lasergene Software Suite v.7.1.0 (Madison, WI).

The sCJD patients included 129 MM (2), MV (3), and VV (1). The four GSS-F198S patients had a missense mutation at *PRNP* codon 198 (F198S mutation) and were 129 MV (3) or VV (1). The GSS-P102L case had a missense mutation at *PRNP* codon 102 (P102L) and was 129 MV.

A diagnosis of prion disease was confirmed for all cases by detection of PK-resistant PrP on immunoblots of brain samples. Characterization of sCJD prion subtype was based on PrP^{Sc} electrophoretic mobility and *PRNP* genotype. All four GSS-F198S patient brain samples showed 8 kDa and higher molecular weight PrP bands by immunoblot, consistent with the published N- and C-terminally truncated PrP fragment ($_{74}$GQPHGGGWGQPHGGGWGQGGGTHSQWNKP$_{102}$) [83] and multicentric plaques histologically, whereas the GSS-P102L case showed a ≈21 kDa (type 1) PrP band and no lower molecular weight bands, as well as diffuse, synaptic PrP deposits in the cerebral cortex, and multicentric plaques in the cerebellum, similar to a subset of GSS-P102L cases previously published [78].

Purification of PrP^{Sc} for structural studies by mass spectrometry

Samples were purified from mouse (whole brain) and human brain (cerebellum: GSS-F198S, sCJD MM1 and sCJD MV1, frontal cortex: GSS-P102L and sCJD MM2, and occipital cortex: sCJD MM1) as previously described [89] with minor modifications. One ml of 10% brain homogenate in PBS (w/v) was mixed with an equal volume of TEN(D) buffer (5% sarkosyl in 50 mM Tris-HCl, 5 mM EDTA, 665 mM NaCl, 0.2 mM dithiothreitol, pH 8.0), containing complete TM protease inhibitors (Roche). Samples were incubated on ice for 1 hour and centrifuged at 18,000 x *g* for 30 minutes at 4 °C. All but 100 μl of supernatant was removed, and the pellet was resuspended in 100 μl of residual supernatant and diluted to 1 ml with 10% sarkosyl TEN(D). Each supernatant and pellet was incubated for 30 minutes on ice and then centrifuged at 18,000 x *g* for 30 minutes at 4 °C. Supernatants were recovered while pellets were held on ice. Supernatants were added separately into ultracentrifuge tubes with 10% sarcosyl TEN(D) buffer containing protease inhibitors and centrifuged at 150,000 x *g* for 2.5 hours at 4 °C. Supernatants were discarded while pellets were rinsed with 100 μl of 10% NaCl in TEN(D) buffer with 1% sulfobetaine (SB 3–14) and protease inhibitors and then combined and centrifuged at 225,000 x *g* for 2 hours at 20 °C. The supernatant was discarded and pellet was washed and then resuspended in ice cold TMS buffer containing protease inhibitors (10 mM Tris-HCl, 5 mM $MgCl_2$, 100 mM NaCl, pH 7.0). Samples were incubated on ice overnight at 4 °C. Samples were then incubated with 25 units/ml benzonase™ (Sigma-Aldrich) and 50 mM $MgCl_2$ for 30 minutes at 37 °C at followed by a digestion with 10 μg/ml PK for 1 hour at 37 °C. PK digestion was stopped by incubating samples with 2 mM PMSF on ice for 15 minutes. Samples were incubated with 20 mM EDTA for 15 minutes at 37 °C. An equal volume of 20% NaCl was added to all tubes followed by an equal volume of 2% SB 3–14 buffer. For the sucrose gradient, a layer of 0.5 M sucrose, 100 mM NaCl, 10 mM Tris, and 0.5% SB 3–14, pH 7.4 was added to ultracentrifuge tubes. Samples were then carefully transferred and the tubes topped with

TMS buffer. Samples were centrifuged at 200,000 x *g* for 2 hours at 20 °C. The pellet was rinsed with 0.5% SB 3–14 in PBS. Pellets were resuspended in 50 μl of 0.5% SB 3–14 in PBS and stored at −80 °C. Gel electrophoresis and silver staining were performed to confirm the purity of the PrP^{Sc}. To quantify PrP levels, samples were compared against a dilution series of recombinant PrP by immunoblotting and probing with POM19 and 3F4 anti-PrP antibodies.

Heparan sulfate purification and analysis by mass spectrometry

The purified PrP^{Sc} samples were digested with 0.5 M NaOH (final concentration) on ice for 16 hours at 4 °C, neutralized with 0.5 M acetic acid (final concentration), and digested with pronase for 25 hours at 37 °C. HS was next extracted by anion exchange chromatography using diethyl-aminoethyl (DEAE) sepharose columns (Healthcare Life Sciences). For depolymerization, HS was extensively digested with 1 milli-unit each of heparinases I, II, and III (AMS Biotechnology). The disaccharides resulting from enzymatic depolymerization were tagged by reductive amination with [$^{12}C_6$]aniline [58, 59]. The [$^{12}C_6$]aniline-tagged disaccharides were mixed with [$^{13}C_6$]aniline-tagged disaccharide standards. Samples were analyzed by liquid chromatography-mass spectrometry (LC-MS) using an LTQ Orbitrap Discovery electrospray ionization mass spectrometer (ThermoFisher Scientific). Internal disaccharides were identified based on their unique mass and quantified relative to the wet weight of tissue [58, 59]. The level of measured HS relative to the PrP^{Sc} level (measured by western blotting with a recombinant PrP dilution series) was calculated and plotted.

Statistics

Log-rank (Mantel-Cox) tests were performed to assess survival differences between groups. A Student's t-test (two-tailed, unpaired) was used to determine the statistical significance between the $Ext1^{+/-}$ and $Ext1^{+/+}$ mouse groups for the PrP^{C} expression level, lesion profiles, activated microglia, PrP^{Sc} glycoprofiles, PrP^{Sc} conformation stability, and PrP^{Sc} fibril structure (FLIM). A non-parametric Fisher's exact test was used to compare the proportion of $Ext1^{+/-}$ versus $Ext1^{+/+}$ mice having plaques by brain region. A two-way ANOVA with Bonferroni's post test was used to compare the number of parenchymal, vascular, and periventricular plaques in $Ext1^{+/-}$ versus $Ext1^{+/+}$ mice, as well as the HS composition associated with different prion strains. A nonparametric Spearman correlation test was used to test the correlation of plaque numbers in the corpus callosum versus velum interpositum within a mouse group ($Ext1^{+/-}$ or $Ext1^{+/+}$). The statistical significance in the level of HS bound to PrP and the level of ADAM10-cleaved PrP among prion strains were determined by performing a non-parametric, two-tailed Wilcoxon rank sum test (when 2 strains were compared) or a one-way ANOVA with Tukey's post test (when three or more strains were compared). For all analyses, $p < 0.05$ was considered significant.

The Wilcoxon test is an exact test, meaning the minimum observable p-value is constrained when the sample size is small. Notably, there were two comparisons (Fig. 4f and 5d) where there was a complete separation of values but nonetheless the exact test p-value did not reach statistical significance. In this circumstance the lack of formal statistical significance should not be interpreted as a null finding.

Study approval

All animal studies were performed following procedures to minimize suffering and were approved by the Institutional Animal Care and Use Committee at UC San Diego. Protocols were performed in strict accordance with good animal practices, as described in the Guide for the Use and Care of Laboratory Animals published by the National Institutes of Health.

This study was approved by the human research protection committees at UC San Francisco and Case Western Reserve University (IRB Study Numbers 10-04905 and 03-14-28, respectively). All brain tissues utilized were deidentified samples collected at autopsy (NIH Office of Human Subjects Research Protections, exemption 4).

RESULTS

HS proteoglycans (HSPG) promote prion internalization and replication *in vitro* [46, 113]. To determine how HS modulates prion infection *in vivo*, we challenged *Ext1*$^{+/-}$ [60] and *Ext1*$^{+/+}$ (WT) littermate control mice with prions. Groups of mice were inoculated intracerebrally with three mouse-adapted prion strains, RML, ME7, and mCWD, or uninfected control brain (mock). mCWD prion infection is prolonged in WT mice (approximately 550 days), therefore *Ext1*$^{+/-}$ mice were bred to *tga*20 mice, which express 4-6 fold higher levels of mouse PrP^{C} [31] and the F1 generation (*tg*a20$^{+/-}$;*Ext1*$^{+/-}$ and *tg*a20$^{+/-}$;*Ext1*$^{+/+}$ mice) was inoculated with mCWD. The PrP^{C} expression in the brain was similar for *Ext1*$^{+/-}$ and *Ext1*$^{+/+}$ mice as well as for *tg*a20$^{+/-}$;*Ext1*$^{+/-}$ and *tg*a20$^{+/-}$;*Ext1*$^{+/+}$ mice (Online resource 1).

Prion disease phenotype triggered by subfibrillar strains is minimally altered in mice expressing short HS chains

Ext1$^{+/-}$ and *Ext1*$^{+/+}$ mice exposed to RML subfibrillar prions showed no difference in the survival time [141 ± 11 versus 145 ± 4 days post-inoculation (dpi), respectively] (Fig. 1a), however *Ext1*$^{+/-}$ mice exposed to ME7 prions showed a modest but significantly prolonged survival [169 ± 7 dpi versus 157 ± 12 dpi (*Ext1*$^{+/-}$ and *Ext1*$^{+/+}$ mice, respectively)] (Fig. 1a). In comparing the two subfibrillar strains histologically, we found that RML prions induce fine to punctate 1 - 5 μm aggregates and ME7 prions induce punctate and small, plaque-like deposits, both accompanied by spongiform change and astrocytic gliosis (Fig. 1b). The prion-infected *Ext1*$^{+/-}$ and *Ext1*$^{+/+}$ mice showed similar aggregate morphologies and affected brain regions within each strain, resulting in nearly overlapping lesion profiles (spongiform change, gliosis, and prion deposition) and indicating no major differences in the histopathology due to the shortened HS chains (Fig. 1c).

To determine whether the biochemical properties of RML and ME7 were altered in mice expressing short HS chains, we compared the electrophoretic mobility, glycoform profile, and PrP^{Sc} level in brain, and found no differences (Fig. 1d,e and Online resource 2). Thus the shorter HS chains in *Ext1*$^{+/-}$ mice do not markedly affect the brain lesions, PrP^{Sc} levels, or the biochemical properties of subfibrillar prions, but led to a modest prolongation in survival following infection with one subfibrillar strain, ME7.

Short HS chains prolong survival and alter the distribution of fibrillar prions

Unlike RML and ME7, mCWD prions form long fibrils visible *in situ* by electron microscopy [95] and accumulate as extracellular plaques containing acidic polysaccharides (Online resource 3). In contrast to the mice infected with subfibrillar prions, *tg*a20$^{+/-}$*Ext1*$^{+/-}$ mice infected with mCWD prions showed a markedly prolonged survival that was more than 30 days longer as compared to the *tg*a20$^{+/-}$*Ext1*$^{+/+}$ mice (275 ± 25 versus 237 ± 37 dpi, respectively) (Fig. 2a), yet with no differences in the total PrP^{Sc} levels at terminal disease (Online resource 2). However, the histopathology in the *tg*a20$^{+/-}$*Ext1*$^{+/-}$ mice was profoundly altered. Most of the *tg*a20$^{+/-}$*Ext1*$^{+/+}$ mice infected with mCWD (80%, 8/10 mice) developed large (50 - 100 μm) extracellular plaques in the corpus callosum (Fig. 2b), as is typical for this prion strain (100% of mCWD-infected *tg*a20 mice, n=11) [12]. In contrast, only approximately 30% (5/16) of *tg*a20$^{+/-}$*Ext1*$^{+/-}$ mice accumulated plaques in the corpus callosum (Fig. 2c), and the plaque number in each mouse was significantly reduced (Fig. 2d). Instead, mCWD prions accumulated within and around blood vessels (amyloid angiopathy) more broadly distributed throughout the brain, including unusual locations rarely observed in the *tg*a20$^{+/-}$*Ext1*$^{+/+}$ mice or in any of the previous mCWD-infected *tg*a20 mice examined, such as the cerebral cortex, basal ganglia, thalamus, and hypothalamus (Fig. 2c and Online resource 4a).

Interestingly, *tg*a20$^{+/-}$*Ext1*$^{+/-}$ brains showed significantly more perivascular plaques in the cerebellum and velum interpositum, a continuum of the subarachnoid space [30], as compared to *tg*a20$^{+/-}$*Ext1*$^{+/+}$ brains (Fig. 2d). In the *tg*a20$^{+/-}$*Ext1*$^{+/+}$ brains, the plaque numbers in the corpus callosum and velum interpositum were inversely correlated ($p < 0.01$, Spearman correlation test), suggesting that with PrP^{Sc} forming fewer parenchymal plaques, deposition occurred instead perivascularly.

We next compared the plaque distribution with survival time in the *tg*a20$^{+/-}$*Ext1*$^{+/-}$ mice and found that the mice that survived the longest (more than 260 dpi) had the most widely distributed plaques, with plaques in the hippocampus, cortex, thalamus, and basal ganglia (Online resource 4b), despite having total plaque numbers that did not significantly vary from the mice with shorter survival times.

The spongiform change and gliosis in the infected *tga20*$^{+/-}$*Ext1*$^{+/-}$ brains closely resembled the *tga20*$^{+/-}$*Ext1*$^{+/+}$ brains (Fig. 2e). The plaques remained congophilic (Fig. 2f) and showed a similar plaque morphology as seen in the *tga20*$^{+/-}$*Ext1*$^{+/+}$ brains (Fig. 2b). Dual immunostaining of brain sections for PrP and endothelial cells revealed that all the plaques in the corpus callosum were parenchymal, whereas nearly all plaques in non-callosal regions were perivascular (*tga20*$^{+/-}$*Ext1*$^{+/+}$: 88% and *tga20*$^{+/-}$*Ext1*$^{+/-}$: 94%) (Fig. 2g). Notably, some plaques were also observed subjacent to the ventricle (*tga20*$^{+/-}$*Ext1*$^{+/+}$: 8% and *tga20*$^{+/-}$*Ext1*$^{+/-}$: 3%).

To determine how the expanded mCWD plaque distribution impacted the neuroinflammatory response, we next measured the level of activated microglia in the brains of *tg*a20$^{+/-}$*Ext1*$^{+/-}$ and *tg*a20$^{+/-}$*Ext1*$^{+/+}$ mice by immunolabelling with ionizing calcium-binding adaptor molecule 1 (Iba1) antibody [47]. The level of microglial activation and clustering around mCWD plaques was indistinguishable between mice at terminal prion

disease (Fig. 2h), suggesting there were no differences in the inflammatory response. Short HS chains could alter the mCWD conformation, which may change the plaque distribution and prolong prion disease. Thus, we next studied whether the mCWD fibril structure differed in *tg*a20$^{+/-}$*Ext1*$^{+/-}$ mice using fluorescence lifetime imaging (FLIM) of h-FTAA stained deposits. h-FTAA is a heptameric oligothiophene that has previously been used to distinguish prion aggregates associated with distinct prion strains [2, 65]. FLIM experiments were conducted with excitation of h-FTAA at 490 nm and the acquired decay curves were fitted with a bi-exponential decay function and two components of the fit. We found that the intensity-weighted mean lifetime (ti) displayed by h-FTAA showed similar distributions for mCWD deposits in *tg*a20$^{+/-}$*Ext1*$^{+/+}$ and *tg*a20$^{+/-}$*Ext1*$^{+/-}$ mice (Fig. 3a). Thus, h-FTAA binds in an analogous fashion to these prion deposits, suggesting that mCWD is not structurally altered in the *tg*a20$^{+/-}$*Ext1*$^{+/-}$ mice. Consistent with this result, the biochemical properties of the mCWD PrP^{Sc} in *tg*a20$^{+/-}$*Ext1*$^{+/+}$ and *tg*a20$^{+/-}$*Ext1*$^{+/-}$ mice, including electrophoretic mobility, glycoprofile, and aggregate stability in GdnHCl, were indistinguishable (Fig. 3b,c), indicating that the altered prion distribution observed with *Ext1* haploinsufficiency was not due to a change in the prion conformation.

mCWD prions are GPI-anchorless

PrP^{C} is tethered to the outer leaflet of the plasma membrane by a GPI–anchor, however, 10-15% of PrP^{C} is constitutively cleaved between Gly228 and Arg229 (murine PrP) by the metalloproteinase ADAM10, releasing nearly full length PrP^{C} from the cell surface [4, 106] (Fig. 4a). Prion aggregates reportedly contain the GPI-anchor [103], yet conformers are diverse and it is possible that not all prions are GPI-anchored. To determine whether mCWD prions harbor a GPI-anchor, we employed a newly developed antibody that recognizes ADAM10-cleaved PrP (sPrP^{G228}) [63] and an antibody that recognizes cleaved and uncleaved (total) PrP (POM19) [85]. We found that abundant mCWD PrP^{Sc}, yet minimal RML and ME7 PrP^{Sc}, were recognized by the sPrP^{G228} antibody, indicating that PK-resistant mCWD is largely composed of ADAM10-cleaved PrP lacking the the GPI-anchor and three C-terminal amino acid residues (Fig. 4b). The level of ADAM10-cleaved PrP^{Sc} correlated with the plaque morphology among the three strains, as mCWD had the highest ratio of GPI-anchorless PrP^{Sc} to total PrP^{Sc} signal (630) and showed 100% extracellular plaques. In contrast, RML and ME7 had lower ratios (0.36 and 3.25, respectively) (Fig. 4c) and no or few extracellular plaques, respectively, consistent with being GPI-anchored as previously reported for PrP^{Sc}[67, 104]. To localize the ADAM10-cleaved PrP^{Sc} in mCWD-infected brain, we performed immunostaining on brain sections using the sPrP^{G228} antibody. These experiments revealed strong immunolabelling of mCWD plaques, indicating GPI-anchorless PrP forms plaques of near full length PrP. Conversely, there was very weak immunolabelling of RML aggregates (Fig. 4d).

GPI-anchorless prions contain high levels of HS

We reasoned that the GPI-anchorless state may enable shed PrP^{C} and small prion aggregates to better interact with HS in the extracellular matrix. In this case, GPI-anchorless prions would be predicted to have more HS bound. To compare the levels of HS bound to GPI-anchored and -anchorless prions, we utilized two GPI-anchored (sPrP^{G228} negative), subfibrillar prion strains, RML and 22L, that had been serially passaged in transgenic mice

expressing GPI-anchorless PrP [tg(GPI-PrP)] [21], generating GPI-anchorless RML and 22L (22L shown in Online resource 3 and 5). In the GPI-anchorless state, RML and 22L prions are fibrillar and vasculotropic [3], as originally reported by Chesebro and colleagues for RML [21]. We purified the GPI-anchored and anchorless prions from brain, assessed the PrP^{Sc} purity by silver stain (Online resource 6), quantified the PrP^{Sc} levels, measured the HS levels by liquid chromatography-mass spectrometry (LC-MS), and calculated the HS : PrP^{Sc} ratio. Remarkably, we found approximately 20-fold more HS bound to GPI-anchorless RML and 22L prions as compared to GPI-anchored RML and 22L (Fig. 4e,f). Furthermore, upon testing mCWD prions we also found relatively high levels of HS bound (Fig. 4f), consistent with the other GPI-anchorless prions.

Although the LC-MS was performed on highly purified prion preparations, it is possible that HS associates with PrP during the isolation process. To further investigate the association of HS and PrP, we localized PrP and HS in brain sections from mCWD-infected *tg*a20$^{+/-}$*Ext1*$^{+/+}$ and *tg*a20$^{+/-}$*Ext1*$^{+/-}$ by dual immunolabelling *in situ*. Supporting the *in vivo* binding of PrP and HS, we found that HS intensely co-labelled with prion plaques, whereas the heparinase-digested (Fig. 4g) and isotype control samples were HS negative. HS and PrP single stains confirmed antibody specificity. We found that parenchymal plaques consistently showed strong HS immunolabelling (100%, n=35 plaques).

The GPI-anchorless prions consistently had exceedingly more HS bound than their GPI-anchored counterparts, suggesting that GPI-anchored prions rarely or only transiently interact with HS. We reasoned that adding a GPI-anchor onto mCWD should create a prion that binds less HS. Therefore we next tested a recently developed *GPI-anchored* mCWD strain obtained by passaging GPI-anchorless mCWD into *tg*a20 mice (new mCWD) [3] (Fig. 5a-c). The new GPI-anchored mCWD formed diffuse deposits in the corpus callosum and hippocampus, and no longer formed plaques, bound Congo red, or stained strongly with Alcian blue (Fig. 5a). We performed LC-MS on prion-bound HS isolated from the brains of mice infected with GPI-anchorless mCWD prions (tg(GPI-PrP) mice) and the new GPI-anchored mCWD prions (*tg*a20 mice) to compare with the original ADAM10-cleaved mCWD. Strikingly, while the ADAM10-cleaved mCWD and GPI-anchorless mCWD prions had abundant HS bound, the new GPI-anchored mCWD prions resembled other GPI-anchored prions in consistently showing very low levels of HS bound (Fig. 5d,e), supporting earlier findings that GPI-anchored prions harbor less HS. Interestingly, the HS disaccharide composition was somewhat similar between the ADAM10-cleaved mCWD and the new GPI-anchored mCWD, yet differed from the GPI-anchorless mCWD, as HS was generally more sulfated in the GPI-anchorless mCWD, specifically in the level of N-sulfated and 2-O sulfated HS (Fig. 5f and Online resource Table 1). In HS-immunolabelled brain sections, we also found that HS co-localized with ADAM10-cleaved and GPI-anchorless mCWD, but not with the new GPI-anchored mCWD prions, indicating that HS mainly accumulates in extracellular, fibrillar prion plaques (Fig. 5g).

Human plaque forming prions also bind abundant HS

In certain human familial prion diseases, particularly Gerstmann-Sträussler-Scheinker (GSS) disease, N- and C-terminally cleaved, GPI-anchorless PrP forms parenchymal plaques or

perivascular amyloid [35-38, 48, 83, 116], whereas in other diseases, near full length to full length PrP forms fine granular synaptic deposits and plaque-like deposits [50]. To test whether human plaque-forming prions also bind significantly more HS than the non-plaque forming prions, we used LC-MS to measure the prion-bound HS levels and composition in post-mortem brain samples from eleven patients diagnosed with familial or sporadic prion disease. The familial cases consisted of five patients having missense mutations in codon 198 (F198S) or codon 102 (P102L) of *PRNP*. The six sCJD cases were previously characterized by subtype [74], and consisted of subtypes MM1 (2), MV1 (1), MV2K (2), and VV2 (1) (Table 1).

Four of the patients with familial prion disease (GSS-F198S) had developed compact multicentric PrP plaques involving deep layers of the neocortex and subpial regions with no spongiform degeneration (Online resource 7). Confluent plaques were identified throughout the gray matter structures within the basal ganglia, thalamus, midbrain, cerebellar molecular layer and dentate nuclei. PK-resistant PrP fragments of 8 kDa and higher were detected by immunoblotting (Fig. 6a), consistent with published reports [24, 25, 37, 38, 44, 84]. The fifth familial case (GSS-P102L) developed moderate, full-thickness spongiform degeneration with synaptic deposits (no plaques) throughout the cortex (Online resource 7) and scattered pleomorphic unicentric and multicentric plaques and plaque-like deposits in the cerebellum and thalamus. Immunoblotting of the frontal cortex revealed PK-resistant PrP composed of 3 bands from ~21 kDa to 30 kDa, similar to PrP from sCJD MM1 cases although with a different glycoform ratio (Fig. 6a), consistent with a previously published study [78].

The three sCJD cases with rapidly progressive disease (1.6 to 6 months) (MM1 and MV1) histologically showed a moderate degree of spongiform change with small, sometimes confluent vacuoles and fine granular and synaptic PrP aggregates (Online resource 7). PK-resistant PrP having an electrophoretic mobility of 21 kDa (unglycosylated PrP) was detected by immunoblot (Fig. 6a). The MV2 and VV2 cases histologically were characterized by mild spongiform change (MV2) or focal areas of spongiform change (VV2) and diffuse aggregates as well as small plaques and plaque-like deposits (Online resource 7 and Table 1). Upon immunoblotting, PK-resistant bands were present at 19 and 20 kDa or 19 kDa, respectively (Fig. 6a).

Consistent with the results in mice, mass spectrometry of HS bound to PrP purified from the human brain samples revealed abundant HS bound to the plaque-forming prions (GSS-F198S cases), with approximately 10- to 100-fold higher HS levels than HS present in the seven cases having plaque-like deposits (sCJD) or diffuse deposits [sCJD and GSS-P102L (cortex)], respectively (Fig. 6b,c). Remarkably, the lowest HS levels (~100-fold lower than GSS-F198S) were associated with the diffuse prion aggregates [sCJD MM1 and MV1 and GSS-P102L (cortex)], while intermediate levels of HS (~10-fold lower) were associated with the sCJD cases having small plaques and plaque-like deposits (VV2 and MV2K) (Fig. 6c). Thus the HS levels once again correlated with the presence of plaques or plaque-like deposits in the brain.

Notably, the composition of the HS bound to the multicentric plaque-forming GSS prions was similar to that bound to sCJD prions. The primary differences were in the relatively low levels of unsulfated N-acetylated HS and 6-O sulfated HS in the GSS-F198S cases as compared to the sCJD cases (Fig. 6d).

To localize the abundant HS detected in the GSS-F198S cases in tissue sections, we next immunolabelled brain sections and found intense HS labelling concentrated in the plaque core (Fig. 6e), reported to contain the N- and C-terminally truncated PrP [38]. This finding indicates that HS binds prion plaques in human brain parenchyma, and less so to the synaptic and punctate deposits, consistent with the findings in the prion-infected mice.

DISCUSSION

Here we provide the first *in vivo* evidence of an endogenous co-factor, HS, that facilitates parenchymal prion plaque deposition in the brain. mCWD prion-infected mice with *Ext1* haploinsufficiency showed fewer parenchymal plaques, an increase in vascular plaques, and a prolonged survival time. In addition, we found that the mCWD plaques were composed of ADAM10-cleaved, extracellular PrP and exceedingly high levels of HS, particularly 6-O-sulfated HS. Although mCWD-infected *tg*a20$^{+/-}$;*Ext1*$^{+/-}$ mice showed a longer survival time, there was no evidence for a change in the prion conformation, biochemically or histologically, implicating a role for HS in the altered plaque distribution. Taken together, our studies suggest that HS binds shed, GPI-anchorless prion protein and enhances parenchymal plaque formation, potentially through scaffolding prion fibril assembly and reducing prion transit toward blood vessels.

Surprisingly, *Ext1* haploinsufficiency led to either a modest or no change in the disease progression induced by GPI-anchored, subfibrillar prions. This remarkable and unexpected finding suggests little or only a transient interaction between HS and GPI-anchored prions, in stark contrast to the GPI-anchorless prions. We found a strong correlation between the GPI-anchored state of the prion and the level of HS bound, suggesting that GPI-anchorless prions interact more frequently with HS or with higher affinity. Mobile, GPI-anchorless prions in mice and humans typically form parenchymal plaques or cerebral amyloid angiopathy (CAA), depending on the specific mutation [21, 36, 48, 90]. Here we found that two GPI-anchorless prion strains (GPI$^-$ RML and GPI$^-$ 22L) bound abundant HS, whereas their GPI-anchored counterparts bound very little. Additionally, while ADAM10-cleaved, GPI-anchorless mCWD prions bound abundant HS, the new GPI-anchored mCWD prions bound very little HS. Our results suggest that GPI-anchoring of prions to the cell membrane topologically constrains prions, limiting access and binding to extracellular HS. Thus we propose two key factors tightly linked to the formation of parenchymal plaques in prion disease that ultimately impact the disease phenotype: (1) mobile, GPI-anchorless PrP and (2) extracellular HS.

The modest effect of *Ext1* haploinsufficiency on GPI-anchored prion disease seemingly contradicts previous studies that HS or heparin binds and promotes PrP internalization and conversion *in vitro* [7, 42, 46, 77, 94]. *In vitro*, exogenously applied sulfated polyanions were shown to reduce prion replication in cells, potentially by inhibiting prion binding to

endogenous HS [19]. Additionally, heparanase overexpression in RML-infected mice infected led to a prolonged survival time [54], however the impact on prion aggregate conformation and brain distribution were not described. Here HS chains were shortened but not eliminated, therefore we cannot exclude a role for HS chains in advancing GPI-anchored prion disease. Further *in vivo* work using additional enzyme mutants involved in HS synthesis would be required to better understand how cell surface HS impacts GPI-anchored prion disease.

The mCWD plaque redistribution to perivascular sites and the delay in disease observed in the *Ext1*$^{+/-}$ mice are reminiscent of findings from an Alzheimer's disease mouse model (APP/PS1) deficient in neuronal HS chains, which showed a marked reduction in amyloid-β parenchymal plaques and an increased amyloid angiopathy compared to aged-match APP/PS1 mice [64]. Interestingly, clearance of the amyloid-β monomer was increased in mice lacking neuronal HS [64], suggesting that HS may trap amyloid-β in the parenchyma and prevent clearance by bulk fluid flow. In human brain, HS proteoglycans co-localize with amyloid-β plaques [97, 108], similar to what we observed in the familial prion disease cases with plaques (F198S). Thus, HS may be a fundamental component in parenchymal fibril assembly common to a subset of prion diseases and Alzheimer's disease. Future mass spectrometry studies may inform on the HS composition in the amyloid-β plaques, enabling further comparison with the prion-bound HS.

The mass spectrometry studies reported here are the first to quantify the levels and composition of HS tightly bound to any amyloidogenic protein in the brain. The findings show striking differences among the prion strains. For example, in comparing the GPI-anchored and -anchorless mCWD conformers, we noted significantly higher levels of N-acetylated and 6-O sulfated HS obtained from the anchorless prions. It has been previously shown that HS sulfation plays a role in the internalization and assembly of prions, tau, amyloid-β, and α-synuclein [45, 46, 88, 105]. Additionally, sulfated GAGs stimulate prion conversion *in vitro* [46]. Our detection of major variation in the prion-associated HS among strains suggests either differences in the affinity of a prion fold for a particular HS structure or in the HS molecules synthesized near the prion deposition site. These findings underscore the need to define the HS structures in different brain regions as well as the molecular determinants for HS binding to protein aggregates.

Collectively, these studies suggest that HS binds shed, GPI-anchorless prions in the parenchyma, but does HS scaffold prions, accelerating fibril assembly and plaque formation? HS chains are abundant, long flexible polymers that are highly anionic and typically act as a scaffold, with electrostatic interactions being major contributors to protein binding [15, 73, 93]. HS chains normally tether and locally concentrate proteins [27, 114], foster protein homo-oligomerization [81, 115], and stabilize extracellular proteins against proteolytic degradation [92], all of which would promote prion assembly. In gelsolin fibril assembly, HS is not required for the nucleation phase, but instead promotes the extension phase, possibly by binding and scaffolding oligomers for conversion into fibrils [99]. In prion assembly, Ma and colleagues found that cofactors were required for recombinant prion protein to form a fibrillar conformation that was both infectious and pathogenic [111]. We suggest that prions co-opt HS as an endogenous co-factor post-nucleation, which facilitates

fibril assembly, as here ADAM10-cleaved and GPI-anchorless prions consistently bound high levels of HS and formed fibrils. Nevertheless, we cannot exclude the possibility that HS passively binds prions post-plaque assembly, although this would not explain the plaque redistribution in the context of the shortened HS chains.

The present findings may help explain the extraordinarily rapid progression of most prion diseases, as the majority are subfibrillar. Diffuse, subfibrillar prion deposits (noncongophilic) correlate with rapidly progressive disease, whereas plaque-forming, fibrillar prions (congophilic) tend to correlate with longer, more slowly progressive disease, with some exceptions. Patients with sporadic CJD (subtype MM1 or MV1) or familial CJD (fCJD), from missense mutations in codon 200 (E200K) [101] or 208 (R208H) [91] in *PRNP*, typically develop subfibrillar aggregates (synaptic, granular, and plaque-like deposits) and show a short survival time of less than 1 year [32, 51], whereas patients with PrP cerebral amyloidosis, for example, from missense or nonsense mutations in codon 102 (P102L) [43, 55, 112], 145 (Y145X), 226 (Y226X, or 227 (Q227X) in *PRNP* [36, 48], develop parenchymal or vascular amyloid and show a longer survival time, with a mean of five years [34, 51]. How HS impacts the kinetics of fibril assembly and ultimately survival time would be worth further study. The rapidly progressive disease in sCJD or fCJD could be explained, in part, by the limited access of GPI-anchored prions to extracellular HS scaffolds, reducing fibril assembly and resulting in primarily subfibrillar aggregates, although whether these aggregates are GPI-anchored in human prion disease is not clear. GPI-anchorless PrP fragments have been detected in the brain of sCJD patients [70]. Our findings also have direct implications for therapy, as interfering with HS binding or modifying endogenous HS structure would be predicted to have the most significant impact on the progression of fibrillar, plaque-forming prion diseases, including GSS. As most systemic amyloids form extracellularly and bind HS, including islet amyloid polypeptide in type 2 diabetes [75], these results also suggest that interfering with HS binding to amyloidogenic proteins may be considered more broadly as a therapeutic strategy for amyloidoses.

Supplementary Material

Refer to Web version on PubMed Central for supplementary material.

Acknowledgements

We thank Chrissa Dwyer and Jessica Lawrence for discussions, Biswa Choudhury, Nazilla Alderson, and Jin Wang for outstanding technical support, and the animal care staff at UC San Diego for excellent animal care. We also thank the UC San Diego GlycoAnalytics Core for the mass spectrometry analysis. The authors are also grateful to the patients' families, the CJD Foundation, referring clinicians, and all the members of the National Prion Disease Pathology Surveillance Center for invaluable technical help. This study was supported by the National Institutes of Health grants NS069566 (CJS), NS076896 (CJS), NS103848 (JGS), AG061251 (PAC), the U.S. Centers for Disease Control and Prevention (BA), the CJD Foundation (CJS and HCA), the Werner-Otto-Stiftung (HCA), and the Ramón Areces Foundation (PAC).

REFERENCES

1. Adjou KT, Simoneau S, Sales N, Lamoury F, Dormont D, Papy-Garcia D, Barritault D, Deslys JP, Lasmezas CI (2003) A novel generation of heparan sulfate mimetics for the treatment of prion diseases. J Gen Virol 84: 2595–2603 [PubMed: 12917481]

2. Aguilar-Calvo P, Bett C, Sevillano AM, Kurt TD, Lawrence J, Soldau K, Hammarstrom P, Nilsson KPR, Sigurdson CJ (2018) Generation of novel neuroinvasive prions following intravenous challenge. Brain Pathol 28: 999–1011 Doi 10.1111/bpa.12598 [PubMed: 29505163]

3. Aguilar-Calvo P, Xiao X, Bett C, Erana H, Soldau K, Castilla J, Nilsson KP, Surewicz WK, Sigurdson CJ (2017) Post-translational modifications in PrP expand the conformational diversity of prions in vivo. Sci Rep 7: 43295 Doi 10.1038/srep43295 [PubMed: 28272426]

4. Altmeppen HC, Prox J, Krasemann S, Puig B, Kruszewski K, Dohler F, Bernreuther C, Hoxha A, Linsenmeier L, Sikorska B et al. (2015) The sheddase ADAM10 is a potent modulator of prion disease. eLife 4: Doi 10.7554/eLife.04260

5. Ancsin JB (2003) Amyloidogenesis: historical and modern observations point to heparan sulfate proteoglycans as a major culprit. Amyloid 10: 67–79

6. Bazar E, Jelinek R (2010) Divergent heparin-induced fibrillation pathways of a prion amyloidogenic determinant. ChemBioChem 11: 1997–2002 Doi 10.1002/cbic.201000207 [PubMed: 20799315]

7. Ben-Zaken O, Tzaban S, Tal Y, Horonchik L, Esko JD, Vlodavsky I, Taraboulos A (2003) Cellular heparan sulfate participates in the metabolism of prions. J Biol Chem 278: 40041–40049 Doi 10.1074/jbc.M301152200 [PubMed: 12871949]

8. Beringue V, Le Dur A, Tixador P, Reine F, Lepourry L, Perret-Liaudet A, Haik S, Vilotte JL, Fontes M, Laude H (2008) Prominent and persistent extraneural infection in human PrP transgenic mice infected with variant CJD. PLoS One 3: e1419 Doi 10.1371/journal.pone.0001419 [PubMed: 18183299]

9. Bessen RA, Kocisko DA, Raymond GJ, Nandan S, Lansbury PT, Caughey B (1995) Non-genetic propagation of strain-specific properties of scrapie prion protein. Nature 375: 698–700 [PubMed: 7791905]

10. Bett C, Fernandez-Borges N, Kurt TD, Lucero M, Nilsson KP, Castilla J, Sigurdson CJ (2012) Structure of the beta2-alpha2 loop and interspecies prion transmission. FASEB J 26: 2868–2876 Doi 10.1096/fj.11-200923 [PubMed: 22490928]

11. Bett C, Kurt TD, Lucero M, Trejo M, Rozemuller AJ, Kong Q, Nilsson KP, Masliah E, Oldstone MB, Sigurdson CJ (2013) Defining the conformational features of anchorless, poorly neuroinvasive prions. PLoS Pathog 9: e1003280 Doi 10.1371/journal.ppat.1003280 [PubMed: 23637596]

12. Bett C, Lawrence J, Kurt TD, Orru C, Aguilar-Calvo P, Kincaid AE, Surewicz WK, Caughey B, Wu C, Sigurdson CJ (2017) Enhanced neuroinvasion by smaller, soluble prions. Acta neuropathologica communications 5: 32 Doi 10.1186/s40478-017-0430-z [PubMed: 28431576]

13. Bruce ME (2003) TSE strain variation. Br Med Bull 66: 99–108 [PubMed: 14522852]

14. Calamai M, Kumita JR, Mifsud J, Parrini C, Ramazzotti M, Ramponi G, Taddei N, Chiti F, Dobson CM (2006) Nature and significance of the interactions between amyloid fibrils and biological polyelectrolytes. Biochemistry 45: 12806–12815 Doi 10.1021/bi0610653 [PubMed: 17042499]

15. Capila I, Linhardt RJ (2002) Heparin-protein interactions. Angew Chem Int Ed Engl 41: 391–412 [PubMed: 12491369]

16. Castillo GM, Ngo C, Cummings J, Wight TN, Snow AD (1997) Perlecan binds to the beta-amyloid proteins (A beta) of Alzheimer's disease, accelerates A beta fibril formation, and maintains A beta fibril stability. J Neurochem 69: 2452–2465 [PubMed: 9375678]

17. Caughey B, Brown K, Raymond GJ, Katzenstein GE, Thresher W (1994) Binding of the protease-sensitive form of PrP (prion protein) to sulfated glycosaminoglycan and congo red [corrected] [published erratum appears in J Virol 1994 Jun;68(6):4107]. J Virol 68: 2135–2141 [PubMed: 7511169]

18. Caughey B, Raymond GJ (1991) The scrapie-associated form of PrP is made from a cell surface precursor that is both protease- and phospholipase-sensitive. J Biol Chem 266: 18217–18223 [PubMed: 1680859]

19. Caughey B, Raymond GJ (1993) Sulfated polyanion inhibition of scrapie-associated PrP accumulation in cultured cells. J Virol 67: 643–650 [PubMed: 7678300]

20. Caughey BW, Dong A, Bhat KS, Ernst D, Hayes SF, Caughey WS (1991) Secondary structure analysis of the scrapie-associated protein PrP 27-30 in water by infrared spectroscopy [published

erratum appears in Biochemistry 1991 Oct 29;30(43):10600]. Biochemistry 30: 7672–7680 [PubMed: 1678278]

21. Chesebro B, Trifilo M, Race R, Meade-White K, Teng C, LaCasse R, Raymond L, Favara C, Baron G, Priola S et al. (2005) Anchorless prion protein results in infectious amyloid disease without clinical scrapie. Science 308: 1435–1439 [PubMed: 15933194]
22. Chiti F, Dobson CM (2006) Protein misfolding, functional amyloid, and human disease. Annu Rev Biochem 75: 333–366 [PubMed: 16756495]
23. Cohlberg JA, Li J, Uversky VN, Fink AL (2002) Heparin and other glycosaminoglycans stimulate the formation of amyloid fibrils from alpha-synuclein in vitro. Biochemistry 41: 1502–1511 [PubMed: 11814343]
24. Cracco L, Xiao X, Nemani SK, Lavrich J, Cali I, Ghetti B, Notari S, Surewicz WK, Gambetti P (2019) Gerstmann-Straussler-Scheinker disease revisited: accumulation of covalently-linked multimers of internal prion protein fragments. Acta neuropathologica communications 7: 85 Doi 10.1186/s40478-019-0734-2 [PubMed: 31142381]
25. Dlouhy SR, Hsiao K, Farlow MR, Foroud T, Conneally PM, Johnson P, Prusiner SB, Hodes ME, Ghetti B (1992) Linkage of the Indiana kindred of Gerstmann-Straussler-Scheinker disease to the prion protein gene. Nat Genet 1: 64–67 [PubMed: 1363809]
26. Doh-ura K, Ishikawa K, Murakami-Kubo I, Sasaki K, Mohri S, Race R, Iwaki T (2004) Treatment of transmissible spongiform encephalopathy by intraventricular drug infusion in animal models. J Virol 78: 4999–5006 [PubMed: 15113880]
27. Duchesne L, Octeau V, Bearon RN, Beckett A, Prior IA, Lounis B, Fernig DG (2012) Transport of fibroblast growth factor 2 in the pericellular matrix is controlled by the spatial distribution of its binding sites in heparan sulfate. PLoS Biol 10: e1001361 Doi 10.1371/journal.pbio.1001361 [PubMed: 22815649]
28. Ehlers B, Diringer H (1984) Dextran sulphate 500 delays and prevents mouse scrapie by impairment of agent replication in spleen. J Gen Virol 65: 1325–1330 [PubMed: 6205119]
29. Farquhar CF, Dickinson AG (1986) Prolongation of scrapie incubation period by an injection of dextran sulphate 500 within the month before or after infection. J Gen Virol 67: 463–473 [PubMed: 2419489]
30. Fenstermacher JD, Ghersi-Egea JF, Finnegan W, Chen JL (1997) The rapid flow of cerebrospinal fluid from ventricles to cisterns via subarachnoid velae in the normal rat. Acta Neurochir Suppl 70: 285–287 [PubMed: 9416348]
31. Fischer M, Rülicke T, Raeber A, Sailer A, Moser M, Oesch B, Brandner S, Aguzzi A, Weissmann C (1996) Prion protein (PrP) with amino-proximal deletions restoring susceptibility of PrP knockout mice to scrapie. EMBO J 15: 1255–1264 [PubMed: 8635458]
32. Geschwind MD (2016) Prion Disease In: Daroff JJ RB, Mazziota JC, & Pomero SL (ed) Bradley's Neurology in Clinical Practice 7th edn. Elsevier/Saunders, City, pp 1365–1379
33. Geschwind MD, Josephs KA, Parisi JE, Keegan BM (2007) A 54-year-old man with slowness of movement and confusion. Neurology 69: 1881–1887 Doi 10.1212/01.wnl.0000290370.14036.69 [PubMed: 17984457]
34. Ghetti B, Dlouhy SR, Giaccone G, Bugiani O, Frangione B, Farlow MR, Tagliavini F (1995) Gerstmann-Straussler-Scheinker disease and the Indiana kindred. Brain Pathol 5: 61–75 [PubMed: 7767492]
35. Ghetti B, Piccardo P, Frangione B, Bugiani O, Giaccone G, Young K, Prelli F, Farlow MR, Dlouhy SR, Tagliavini F (1996) Prion protein amyloidosis. Brain Pathol 6: 127–145 [PubMed: 8737929]
36. Ghetti B, Piccardo P, Spillantini MG, Ichimiya Y, Porro M, Perini F, Kitamoto T, Tateishi J, Seiler C, Frangione Bet al. (1996) Vascular variant of prion protein cerebral amyloidosis with tau-positive neurofibrillary tangles: the phenotype of the stop codon 145 mutation in PRNP. Proc Natl Acad Sci U S A 93: 744–748 [PubMed: 8570627]
37. Ghetti B, Tagliavini F, Giaccone G, Bugiani O, Frangione B, Farlow MR, Dlouhy SR (1994) Familial Gerstmann-Straussler-Scheinker disease with neurofibrillary tangles. Mol Neurobiol 8: 41–48 Doi 10.1007/BF02778006 [PubMed: 7916191]
38. Giaccone G, Verga L, Bugiani O, Frangione B, Serban D, Prusiner SB, Farlow MR, Ghetti B, Tagliavini F (1992) Prion protein preamyloid and amyloid deposits in Gerstmann-Straussler-

Scheinker disease, Indiana kindred [published erratum appears in Proc Natl Acad Sci U S A 1993 Jan 1;90(1):302]. Proc Natl Acad Sci U S A 89: 9349–9353 [PubMed: 1357663]

39. Gibson RM, Meyer AM, Winner D, Archer J, Feyertag F, Ruiz-Mateos E, Leal M, Robertson DL, Schmotzer CL, Quinones-Mateu ME (2014) Sensitive deep-sequencing-based HIV-1 genotyping assay to simultaneously determine susceptibility to protease, reverse transcriptase, integrase, and maturation inhibitors, as well as HIV-1 coreceptor tropism. Antimicrob Agents Chemother 58: 2167–2185 Doi 10.1128/aac.02710-13 [PubMed: 24468782]
40. Hijazi N, Kariv-Inbal Z, Gasset M, Gabizon R (2005) PrPSc incorporation to cells requires endogenous glycosaminoglycan expression. J Biol Chem 280: 17057–17061 [PubMed: 15668233]
41. Holmes BB, DeVos SL, Kfoury N, Li M, Jacks R, Yanamandra K, Ouidja MO, Brodsky FM, Marasa J, Bagchi DP et al. (2013) Heparan sulfate proteoglycans mediate internalization and propagation of specific proteopathic seeds. Proc Natl Acad Sci U S A 110: E3138–3147 Doi 10.1073/pnas.1301440110 [PubMed: 23898162]
42. Horonchik L, Tzaban S, Ben-Zaken O, Yedidia Y, Rouvinski A, Papy-Garcia D, Barritault D, Vlodavsky I, Taraboulos A (2005) Heparan sulfate is a cellular receptor for purified infectious prions. J Biol Chem 280: 17062–17067 [PubMed: 15668247]
43. Hsiao K, Baker HF, Crow TJ, Poulter M, Owen F, Terwilliger JD, Westaway D, Ott J, Prusiner SB (1989) Linkage of a prion protein missense variant to Gerstmann-Sträussler syndrome. Nature 338: 342–345 [PubMed: 2564168]
44. Hsiao K, Dlouhy SR, Farlow MR, Cass C, Da Costa M, Conneally PM, Hodes ME, Ghetti B, Prusiner SB (1992) Mutant prion proteins in Gerstmann-Straussler-Scheinker disease with neurofibrillary tangles. Nat Genet 1: 68–71 [PubMed: 1363810]
45. Ihse E, Yamakado H, van Wijk XM, Lawrence R, Esko JD, Masliah E (2017) Cellular internalization of alpha-synuclein aggregates by cell surface heparan sulfate depends on aggregate conformation and cell type. Sci Rep 7: 9008 Doi 10.1038/s41598-017-08720-5 [PubMed: 28827536]
46. Imamura M, Tabeta N, Kato N, Matsuura Y, Iwamaru Y, Yokoyama T, Murayama Y (2016) Heparan Sulfate and Heparin Promote Faithful Prion Replication in Vitro by Binding to Normal and Abnormal Prion Proteins in Protein Misfolding Cyclic Amplification. J Biol Chem 291: 26478–26486 Doi 10.1074/jbc.M116.745851 [PubMed: 27821590]
47. Ito D, Imai Y, Ohsawa K, Nakajima K, Fukuuchi Y, Kohsaka S (1998) Microglia-specific localisation of a novel calcium binding protein, Iba1. Brain Res Mol Brain Res 57: 1–9 [PubMed: 9630473]
48. Jansen C, Parchi P, Capellari S, Vermeij AJ, Corrado P, Baas F, Strammiello R, van Gool WA, van Swieten JC, Rozemuller AJ (2010) Prion protein amyloidosis with divergent phenotype associated with two novel nonsense mutations in PRNP. Acta Neuropathol 119: 189–197 Doi 10.1007/s00401-009-0609-x [PubMed: 19911184]
49. Kascsak RJ, Rubenstein R, Merz PA, Tonna DeMasi M, Fersko R, Carp RI, Wisniewski HM, Diringer H (1987) Mouse polyclonal and monoclonal antibody to scrapie-associated fibril proteins. J Virol 61: 3688–3693 [PubMed: 2446004]
50. Kim MO, Cali I, Oehler A, Fong JC, Wong K, See T, Katz JS, Gambetti P, Bettcher BM, Dearmond SJ et al. (2013) Genetic CJD with a novel E200G mutation in the prion protein gene and comparison with E200K mutation cases. Acta neuropathologica communications 1: 80 Doi 10.1186/2051-5960-1-80 [PubMed: 24330864]
51. Kim MO, Takada LT, Wong K, Forner SA, Geschwind MD (2018) Genetic PrP Prion Diseases. Cold Spring Harb Perspect Biol 10: Doi 10.1101/cshperspect.a033134
52. Klingeborn M, Race B, Meade-White KD, Rosenke R, Striebel JF, Chesebro B (2011) Crucial role for prion protein membrane anchoring in the neuroinvasion and neural spread of prion infection. J Virol 85: 1484–1494 Doi 10.1128/JVI.02167-10 [PubMed: 21123371]
53. Kong Q, Zheng M, Casalone C, Qing L, Huang S, Chakraborty B, Wang P, Chen F, Cali I, Corona C et al. (2008) Evaluation of the human transmission risk of an atypical bovine spongiform encephalopathy prion strain. J Virol 82: 3697–3701 Doi 10.1128/JVI.02561-07 [PubMed: 18234793]

54. Kovalchuk Ben-Zaken O, Nissan I, Tzaban S, Taraboulos A, Zcharia E, Matzger S, Shafat I, Vlodavsky I, Tal Y (2015) Transgenic over-expression of mammalian heparanase delays prion disease onset and progression. Biochem Biophys Res Commun 464: 698–704 Doi 10.1016/j.bbrc.2015.06.170 [PubMed: 26168721]
55. Kretzschmar HA, Honold G, Seitelberger F, Feucht M, Wessely P, Mehraein P, Budka H (1991) Prion protein mutation in family first reported by Gerstmann, Straussler, and Scheinker [letter]. Lancet 337: 1160 [PubMed: 1674033]
56. Ladogana A, Casaccia P, Ingrosso L, Cibati M, Salvatore M, Xi YG, Masullo C, Pocchiari M (1992) Sulphate polyanions prolong the incubation period of scrapie-infected hamsters. J Gen Virol 73: 661–665 [PubMed: 1372039]
57. Larramendy-Gozalo C, Barret A, Daudigeos E, Mathieu E, Antonangeli L, Riffet C, Petit E, Papy-Garcia D, Barritault D, Brown P et al. (2007) Comparison of CR36, a new heparan mimetic, and pentosan polysulfate in the treatment of prion diseases. J Gen Virol 88: 1062–1067 Doi 10.1099/vir.0.82286-0 [PubMed: 17325382]
58. Lawrence R, Brown JR, Al-Mafraji K, Lamanna WC, Beitel JR, Boons GJ, Esko JD, Crawford BE (2012) Disease-specific non-reducing end carbohydrate biomarkers for mucopolysaccharidoses. Nat Chem Biol 8: 197–204 Doi 10.1038/nchembio.766 [PubMed: 22231271]
59. Lawrence R, Olson SK, Steele RE, Wang L, Warrior R, Cummings RD, Esko JD (2008) Evolutionary differences in glycosaminoglycan fine structure detected by quantitative glycan reductive isotope labeling. J Biol Chem 283: 33674–33684 Doi 10.1074/jbc.M804288200 [PubMed: 18818196]
60. Lin X, Wei G, Shi Z, Dryer L, Esko JD, Wells DE, Matzuk MM (2000) Disruption of gastrulation and heparan sulfate biosynthesis in EXT1-deficient mice. Dev Biol 224: 299–311 Doi 10.1006/dbio.2000.9798 [PubMed: 10926768]
61. Lindahl B, Lindahl U (1997) Amyloid-specific heparan sulfate from human liver and spleen. J Biol Chem 272: 26091–26094 Doi 10.1074/jbc.272.42.26091 [PubMed: 9334172]
62. Lindahl B, Westling C, Gimenez-Gallego G, Lindahl U, Salmivirta M (1999) Common binding sites for beta-amyloid fibrils and fibroblast growth factor-2 in heparan sulfate from human cerebral cortex. J Biol Chem 274: 30631–30635 [PubMed: 10521448]
63. Linsenmeier L, Mohammadi B, Wetzel S, Puig B, Jackson WS, Hartmann A, Uchiyama K, Sakaguchi S, Endres K, Tatzelt J et al. (2018) Structural and mechanistic aspects influencing the ADAM10-mediated shedding of the prion protein. Mol Neurodegener 13: 18 Doi 10.1186/s13024-018-0248-6 [PubMed: 29625583]
64. Liu CC, Zhao N, Yamaguchi Y, Cirrito JR, Kanekiyo T, Holtzman DM, Bu G (2016) Neuronal heparan sulfates promote amyloid pathology by modulating brain amyloid-beta clearance and aggregation in Alzheimer's disease. Sci Transl Med 8: 332ra344 Doi 10.1126/scitranslmed.aad3650
65. Magnusson K, Simon R, Sjolander D, Sigurdson CJ, Hammarstrom P, Nilsson KP (2014) Multimodal fluorescence microscopy of prion strain specific PrP deposits stained by thiophene-based amyloid ligands. Prion 8: 319–329 Doi 10.4161/pri.29239 [PubMed: 25495506]
66. McBride PA, Wilson MI, Eikelenboom P, Tunstall A, Bruce ME (1998) Heparan sulfate proteoglycan is associated with amyloid plaques and neuroanatomically targeted PrP pathology throughout the incubation period of scrapie-infected mice. Exp Neurol 149: 447–454 [PubMed: 9500966]
67. Naslavsky N, Stein R, Yanai A, Friedlander G, Taraboulos A (1997) Characterization of detergent-insoluble complexes containing the cellular prion protein and its scrapie isoform. J Biol Chem 272: 6324–6331 [PubMed: 9045652]
68. Newman PK, Todd NV, Scoones D, Mead S, Knight RS, Will RG, Ironside JW (2014) Postmortem findings in a case of variant Creutzfeldt-Jakob disease treated with intraventricular pentosan polysulfate. J Neurol Neurosurg Psychiatry 85: 921–924 Doi 10.1136/jnnp-2013-305590 [PubMed: 24554103]
69. Noborn F, O'Callaghan P, Hermansson E, Zhang X, Ancsin JB, Damas AM, Dacklin I, Presto J, Johansson J, Saraiva MJ et al. (2011) Heparan sulfate/heparin promotes transthyretin fibrillization through selective binding to a basic motif in the protein. Proc Natl Acad Sci U S A 108: 5584–5589 Doi 10.1073/pnas.1101194108 [PubMed: 21422279]

70. Notari S, Strammiello R, Capellari S, Giese A, Cescatti M, Grassi J, Ghetti B, Langeveld JP, Zou WQ, Gambetti P et al. (2008) Characterization of truncated forms of abnormal prion protein in Creutzfeldt-Jakob disease. J Biol Chem 283: 30557–30565 Doi 10.1074/jbc.M801877200 [PubMed: 18753138]
71. Nystrom S, Back M, Nilsson KPR, Hammarstrom P (2017) Imaging Amyloid Tissues Stained with Luminescent Conjugated Oligothiophenes by Hyperspectral Confocal Microscopy and Fluorescence Lifetime Imaging. Journal of visualized experiments : JoVE: Doi 10.3791/56279
72. Okada M, Nadanaka S, Shoji N, Tamura J, Kitagawa H (2010) Biosynthesis of heparan sulfate in EXT1-deficient cells. Biochem J 428: 463–471 Doi 10.1042/bj20100101 [PubMed: 20377530]
73. Olson ST, Halvorson HR, Bjork I (1991) Quantitative characterization of the thrombin-heparin interaction. Discrimination between specific and nonspecific binding models. J Biol Chem 266: 6342–6352 [PubMed: 2007587]
74. Orru CD, Soldau K, Cordano C, Llibre-Guerra J, Green AJ, Sanchez H, Groveman BR, Edland SD, Safar JG, Lin JH et al. (2018) Prion Seeds Distribute throughout the Eyes of Sporadic Creutzfeldt-Jakob Disease Patients. mBio 9: Doi 10.1128/mBio.02095-18
75. Oskarsson ME, Singh K, Wang J, Vlodavsky I, Li JP, Westermark GT (2015) Heparan Sulfate Proteoglycans Are Important for Islet Amyloid Formation and Islet Amyloid Polypeptide-induced Apoptosis. J Biol Chem 290: 15121–15132 Doi 10.1074/jbc.M114.631697 [PubMed: 25922077]
76. Pan KM, Baldwin M, Nguyen J, Gasset M, Serban A, Groth D, Mehlhorn I, Huang Z, Fletterick RJ, Cohen FEet al. (1993) Conversion of alpha-helices into beta-sheets features in the formation of the scrapie prion proteins. Proc Natl Acad Sci U S A 90: 10962–10966 Doi 10.1073/pnas.90.23.10962 [PubMed: 7902575]
77. Pan T, Wong BS, Liu T, Li R, Petersen RB, Sy MS (2002) Cell-surface prion protein interacts with glycosaminoglycans. Biochem J 368: 81–90 Doi 10.1042/bj20020773 [PubMed: 12186633]
78. Parchi P, Chen SG, Brown P, Zou W, Capellari S, Budka H, Hainfellner J, Reyes PF, Golden GT, Hauw JJet al. (1998) Different patterns of truncated prion protein fragments correlate with distinct phenotypes in P102L Gerstmann-Straussler-Scheinker disease. Proc Natl Acad Sci U S A 95: 8322–8327 [PubMed: 9653185]
79. Parchi P, Zou W, Wang W, Brown P, Capellari S, Ghetti B, Kopp N, Schulz-Schaeffer WJ, Kretzschmar HA, Head MWet al. (2000) Genetic influence on the structural variations of the abnormal prion protein. Proc Natl Acad Sci U S A 97: 10168–10172. [PubMed: 10963679]
80. Parry A, Baker I, Stacey R, Wimalaratna S (2007) Long term survival in a patient with variant Creutzfeldt-Jakob disease treated with intraventricular pentosan polysulphate. J Neurol Neurosurg Psychiatry 78: 733–734 Doi 10.1136/jnnp.2006.104505 [PubMed: 17314188]
81. Pellegrini L, Burke DF, von Delft F, Mulloy B, Blundell TL (2000) Crystal structure of fibroblast growth factor receptor ectodomain bound to ligand and heparin. Nature 407: 1029–1034 Doi 10.1038/35039551 [PubMed: 11069186]
82. Peretz D, Williamson RA, Legname G, Matsunaga Y, Vergara J, Burton DR, DeArmond SJ, Prusiner SB, Scott MR (2002) A change in the conformation of prions accompanies the emergence of a new prion strain. Neuron 34: 921–932 [PubMed: 12086640]
83. Piccardo P, Liepnieks JJ, William A, Dlouhy SR, Farlow MR, Young K, Nochlin D, Bird TD, Nixon RR, Ball MJet al. (2001) Prion proteins with different conformations accumulate in Gerstmann-Straussler-Scheinker disease caused by A117V and F198S mutations. Am J Pathol 158: 2201–2207 Doi 10.1016/S0002-9440(10)64692-5 [PubMed: 11395398]
84. Piccardo P, Seiler C, Dlouhy SR, Young K, Farlow MR, Prelli F, Frangione B, Bugiani O, Tagliavini F, Ghetti B (1996) Proteinase-K-Resistant Prion Protein Isoforms In Gerstmann-Straussler-Scheinker Disease (Indiana Kindred). J Neuropathol Exp Neurol 55: 1157–1163 [PubMed: 8939199]
85. Polymenidou M, Moos R, Scott M, Sigurdson C, Shi YZ, Yajima B, Hafner-Bratkovic I, Jerala R, Hornemann S, Wuthrich Ket al. (2008) The POM monoclonals: a comprehensive set of antibodies to non-overlapping prion protein epitopes. PLoS One 3: e3872 Doi 10.1371/journal.pone.0003872 [PubMed: 19060956]
86. Prusiner SB (1991) Molecular biology of prion diseases. Science 252: 1515–1522 [PubMed: 1675487]

87. Prusiner SB (1982) Novel proteinaceous infectious particles cause scrapie. Science 216: 136–144 [PubMed: 6801762]

88. Rauch JN, Chen JJ, Sorum AW, Miller GM, Sharf T, See SK, Hsieh-Wilson LC, Kampmann M, Kosik KS (2018) Tau Internalization is Regulated by 6-O Sulfation on Heparan Sulfate Proteoglycans (HSPGs). Sci Rep 8: 6382 Doi 10.1038/s41598-018-24904-z [PubMed: 29686391]

89. Raymond GJ, Chabry J (2004) Methods and Tools in Biosciences and Medicine In: Lehmann S, Grassi J (eds) Techniques in Prion Research. Birkhäuser, Basel, City, pp 16–26

90. Revesz T, Holton JL, Lashley T, Plant G, Frangione B, Rostagno A, Ghiso J (2009) Genetics and molecular pathogenesis of sporadic and hereditary cerebral amyloid angiopathies. Acta Neuropathol 118: 115–130 Doi 10.1007/s00401-009-0501-8 [PubMed: 19225789]

91. Roeber S, Krebs B, Neumann M, Windl O, Zerr I, Grasbon-Frodl EM, Kretzschmar HA (2005) Creutzfeldt-Jakob disease in a patient with an R208H mutation of the prion protein gene (PRNP) and a 17-kDa prion protein fragment. Acta Neuropathol (Berl) 109: 443–448 [PubMed: 15739100]

92. Salanga CL, Handel TM (2011) Chemokine oligomerization and interactions with receptors and glycosaminoglycans: the role of structural dynamics in function. Exp Cell Res 317: 590–601 Doi 10.1016/j.yexcr.2011.01.004 [PubMed: 21223963]

93. Sarrazin S, Lamanna WC, Esko JD (2011) Heparan sulfate proteoglycans. Cold Spring Harb Perspect Biol 3: Doi 10.1101/cshperspect.a004952

94. Shyng SL, Lehmann S, Moulder KL, Harris DA (1995) Sulfated glycans stimulate endocytosis of the cellular isoform of the prion protein, PrPC, in cultured cells. J Biol Chem 270: 30221–30229 [PubMed: 8530433]

95. Sigurdson CJ, Manco G, Schwarz P, Liberski P, Hoover EA, Hornemann S, Polymenidou M, Miller MW, Glatzel M, Aguzzi A (2006) Strain fidelity of chronic wasting disease upon murine adaptation. J Virol 80: 12303–12311 [PubMed: 17020952]

96. Snow AD, Kisilevsky R, Willmer J, Prusiner SB, DeArmond SJ (1989) Sulfated glycosaminoglycans in amyloid plaques of prion diseases. Acta Neuropathol Berl 77: 337–342 [PubMed: 2523631]

97. Snow AD, Mar H, Nochlin D, Kimata K, Kato M, Suzuki S, Hassell J, Wight TN (1988) The presence of heparan sulfate proteoglycans in the neuritic plaques and congophilic angiopathy in Alzheimer's disease. Am J Pathol 133: 456–463 [PubMed: 2974240]

98. Snow AD, Wight TN, Nochlin D, Koike Y, Kimata K, DeArmond SJ, Prusiner SB (1990) Immunolocalization of heparan sulfate proteoglycans to the prion protein amyloid plaques of Gerstmann-Straussler syndrome, Creutzfeldt-Jakob disease and scrapie. Lab Invest 63: 601–611 [PubMed: 1977959]

99. Solomon JP, Bourgault S, Powers ET, Kelly JW (2011) Heparin binds 8 kDa gelsolin cross-beta-sheet oligomers and accelerates amyloidogenesis by hastening fibril extension. Biochemistry 50: 2486–2498 Doi 10.1021/bi101905n [PubMed: 21348501]

100. Spillantini MG, Tolnay M, Love S, Goedert M (1999) Microtubule-associated protein tau, heparan sulphate and alpha-synuclein in several neurodegenerative diseases with dementia. Acta Neuropathol 97: 585–594 [PubMed: 10378377]

101. Spudich S, Mastrianni JA, Wrensch M, Gabizon R, Meiner Z, Kahana I, Rosenmann H, Kahana E, Prusiner SB (1995) Complete penetrance of Creutzfeldt-Jakob disease in Libyan Jews carrying the E200K mutation in the prion protein gene. Mol Med 1: 607–613 [PubMed: 8529127]

102. Staffaroni AM, Elahi FM, McDermott D, Marton K, Karageorgiou E, Sacco S, Paoletti M, Caverzasi E, Hess CP, Rosen HJet al. (2017) Neuroimaging in Dementia. Semin Neurol 37: 510–537 Doi 10.1055/s-0037-1608808 [PubMed: 29207412]

103. Stahl N, Baldwin MA, Burlingame AL, Prusiner SB (1990) Identification of glycoinositol phospholipid linked and truncated forms of the scrapie prion protein. Biochemistry 29: 8879–8884 [PubMed: 1980209]

104. Stahl N, Borchelt DR, Hsiao K, Prusiner SB (1987) Scrapie prion protein contains a phosphatidylinositol glycolipid. Cell 51: 229–240 [PubMed: 2444340]

105. Stopschinski BE, Holmes BB, Miller GM, Manon VA, Vaquer-Alicea J, Prueitt WL, Hsieh-Wilson LC, Diamond MI (2018) Specific glycosaminoglycan chain length and sulfation patterns

are required for cell uptake of tau versus alpha-synuclein and beta-amyloid aggregates. J Biol Chem 293: 10826–10840 Doi 10.1074/jbc.RA117.000378 [PubMed: 29752409]

106. Tagliavini F, Prelli F, Porro M, Salmona M, Bugiani O, Frangione B (1992) A soluble form of prion protein in human cerebrospinal fluid: implications for prion-related encephalopathies. Biochem Biophys Res Commun 184: 1398–1404 [PubMed: 1375461]
107. Todd NV, Morrow J, Doh-ura K, Dealler S, O'Hare S, Farling P, Duddy M, Rainov NG (2005) Cerebroventricular infusion of pentosan polysulphate in human variant Creutzfeldt-Jakob disease. J Infect 50: 394–396 [PubMed: 15907546]
108. van Horssen J, Kleinnijenhuis J, Maass CN, Rensink AA, Otte-Holler I, David G, van den Heuvel LP, Wesseling P, de Waal RM, Verbeek MM (2002) Accumulation of heparan sulfate proteoglycans in cerebellar senile plaques. Neurobiol Aging 23: 537–545 [PubMed: 12009503]
109. Vieira TC, Cordeiro Y, Caughey B, Silva JL (2014) Heparin binding confers prion stability and impairs its aggregation. FASEB J 28: 2667–2676 Doi 10.1096/fj.13-246777 [PubMed: 24648544]
110. Wadsworth JDF, Joiner S, Hill AF, Campbell TA, Desbruslais M, Luthert PJ, Collinge J(2001) Tissue distribution of protease resistant prion protein in variant CJD using a highly sensitive immuno-blotting assay. Lancet 358: 171–180 [PubMed: 11476832]
111. Wang F, Wang X, Yuan CG, Ma J (2010) Generating a prion with bacterially expressed recombinant prion protein. Science 327: 1132–1135 Doi 10.1126/science.1183748 [PubMed: 20110469]
112. Webb TE, Poulter M, Beck J, Uphill J, Adamson G, Campbell T, Linehan J, Powell C, Brandner S, Pal Set al. (2008) Phenotypic heterogeneity and genetic modification of P102L inherited prion disease in an international series. Brain 131: 2632–2646 Doi 10.1093/brain/awn202 [PubMed: 18757886]
113. Wong C, Xiong LW, Horiuchi M, Raymond L, Wehrly K, Chesebro B, Caughey B (2001) Sulfated glycans and elevated temperature stimulate PrP(Sc)-dependent cell-free formation of protease-resistant prion protein. EMBO J 20: 377–386. [PubMed: 11157745]
114. Xu D, Esko JD (2014) Demystifying heparan sulfate-protein interactions. Annu Rev Biochem 83: 129–157 Doi 10.1146/annurev-biochem-060713-035314 [PubMed: 24606135]
115. Xu D, Young JH, Krahn JM, Song D, Corbett KD, Chazin WJ, Pedersen LC, Esko JD (2013) Stable RAGE-heparan sulfate complexes are essential for signal transduction. ACS Chem Biol 8: 1611–1620 Doi 10.1021/cb4001553 [PubMed: 23679870]
116. Zanusso G, Fiorini M, Ferrari S, Meade-White K, Barbieri I, Brocchi E, Ghetti B, Monaco S (2014) Gerstmann-Straussler-Scheinker disease and "anchorless prion protein" mice share prion conformational properties diverging from sporadic Creutzfeldt-Jakob disease. J Biol Chem 289: 4870–4881 Doi 10.1074/jbc.M113.531335 [PubMed: 24398683]

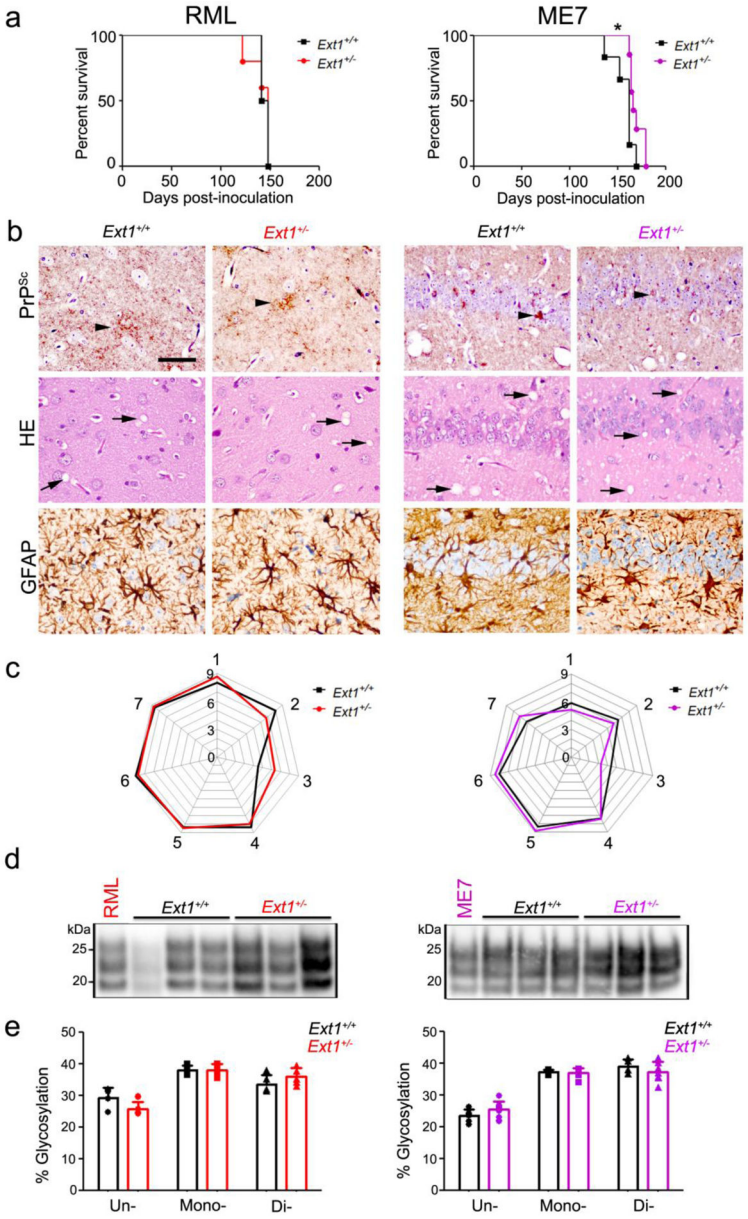

Fig. 1.

Ext1$^{+/+}$ and *Ext1*$^{+/-}$ mice infected with subfibrillar prions show similar survival times, brain lesions, and biochemical properties. **a** A comparison of survival times revealed no differences in RML-infected *Ext1*$^{+/-}$ mice and a modest delay in ME7-infected *Ext1*$^{+/-}$ mice as compared to the *Ext1*$^{+/+}$ mice. **b** Brain sections immunolabelled for PrP and GFAP, or stained with hematoxylin and eosin (HE), show indistinguishable prion aggregate distribution and morphology (arrowheads), spongiform degeneration (arrows), and astrogliosis in *Ext1*$^{+/+}$ and *Ext1*$^{+/-}$ brains. **c** Lesion profiles of RML- and ME7-infected *Ext1*$^{+/+}$ and *Ext1*$^{+/-}$ mice (1-dorsal medulla, 2-cerebellum, 3-hypothalamus, 4-medial thalamus, 5-hippocampus, 6-septum, and 7-cerebral cortex) are almost superimposable. **d** Electrophoretic mobility and **e** glycoprofiles of RML and ME7 strains in *Ext1*$^{+/+}$ and *Ext1*$^{+/-}$ mice. The RML and ME7 inocula were loaded for comparison (first lane). *P< 0.05,

Log-rank (Mantel-Cox) test (panel a). Cerebral cortex (RML) and hippocampus (ME7) shown in panel b. Scale bar = 50 μm (panel b). RML: n=6-7 mice/group; ME7: n=4-5 mice/group.

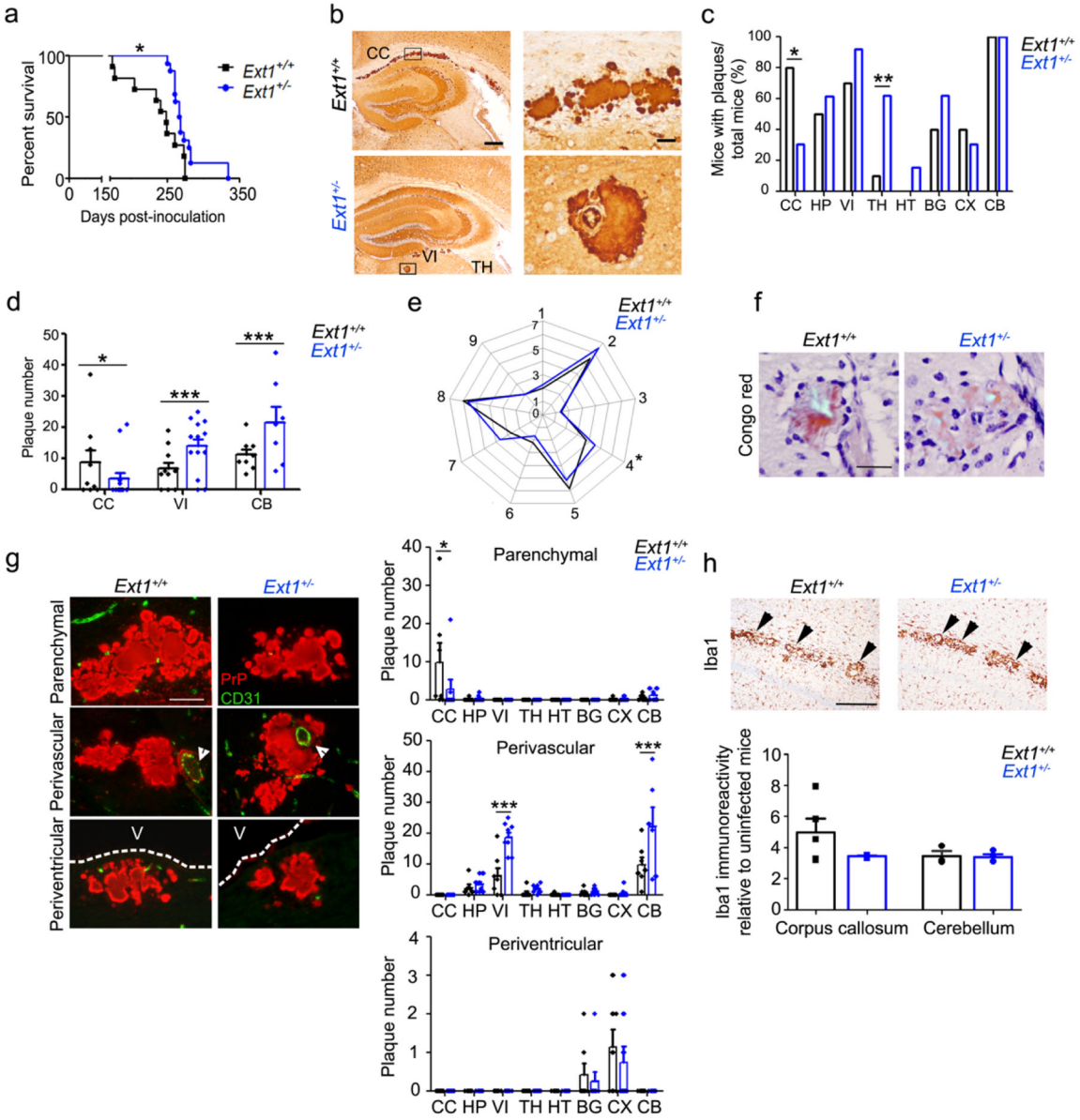

Fig. 2.

mCWD-infected *tg*a20$^{+/-}$*Ext1*$^{+/-}$ mice show prolonged survival times and altered plaque distribution. **a** mCWD-infected *tg*a20$^{+/-}$*Ext1*$^{+/-}$ (“*Ext1*$^{+/-}$”) mice show a significant delay in survival time. **b** PrP immunolabelled brain sections show mCWD prion plaques in the corpus callosum (CC) of *Ext1*$^{+/+}$ mice, whereas in *Ext1*$^{+/-}$ mice, plaques are present in other brain regions including thalamus (TH), and velum interpositum (VI). The plaque morphology was unchanged. **c** The distribution of mCWD plaques varied between the *Ext1*$^{+/+}$ and *Ext1*$^{+/-}$ mice, as fewer *Ext1*$^{+/-}$ mice developed plaques in the corpus callosum (CC), whereas more *Ext1*$^{+/-}$ mice developed plaques in the basal ganglia (BG) and thalamus (TH) (HP: hippocampus, HT: hypothalamus, CX: cerebral cortex, and CB: cerebellum). **d** *Ext1*$^{+/-}$ mice show fewer plaques in the corpus callosum and more plaques in the velum interpositum and cerebellum. **e** Lesion profiles comparing spongiform degeneration,

astrogliosis, and PrP^{Sc} deposition are similar in $Ext1^{+/+}$ and $Ext1^{+/-}$ mice (1-medulla, 2-cerebellum, 3-hypothalamus, 4-medial thalamus, 5-hippocampus, 6-septum, 7-cerebral cortex, 8-cerebral peduncle and 9-cerebellar peduncle). **f** mCWD plaques are congophilic in $Ext1^{+/+}$ and $Ext1^{+/-}$ mice [shown is cerebellum ($Ext1^{+/+}$) and hippocampus ($Ext1^{+/-}$)]. **g** Dual immunostaining for PrP and endothelial cells (CD31) shows typical non-vascular plaques in the corpus callosum (upper panels), perivascular plaques in the basal ganglia, and periventricular plaques adjacent to the lateral ventricle (middle panels, white arrowheads show blood vessel; bottom panels, V=ventricle). $Ext1^{+/-}$ mice show fewer parenchymal plaques in the corpus callosum and more vascular plaques in the velum interpositum and cerebellum. **h** Iba1 immunolabelling of activated microglia shows similar clustering of activated microglia around mCWD plaques in $Ext1^{+/+}$ and $Ext1^{+/-}$ brain sections (arrowheads). Quantification of activated microglia shown in upper panel (for corpus callosum $Ext1^{+/+}$: n= 5 and $Ext1^{+/-}$: n= 3; for cerebellum $Ext1^{+/+}$: n= 3 and $Ext1^{+/-}$: n= 4). Scale bars = 500 μm (left) and 50 μm (right) (panel b), 50 μm (panels f and g), and 1 mm (panel h). *P< 0.05, Log-rank (Mantel-Cox) test (panel a). *P< 0.05, **P< 0.01, ***P< 0.001, Fisher's exact test (panel c), two-way ANOVA with Bonferroni's post test (panels d and g), unpaired, 2-tailed Student's t test (panel e). $Ext1^{+/+}$: n= 11 mice; $Ext1^{+/-}$: n=16 mice.

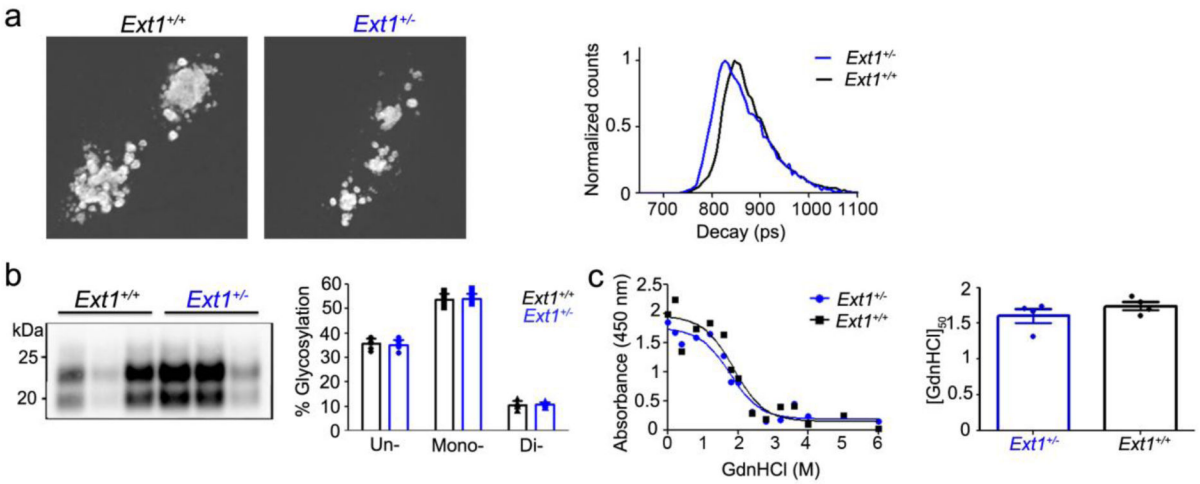

Fig. 3.

mCWD prion conformation is similar in mice having long or short HS chains. **a** h-FTAA fluorescence life-time decay of mCWD prion plaques in *tg*a20$^{+/-}$*Ext1*$^{+/+}$ ("*Ext1*$^{+/+}$") and *tg*a20$^{+/-}$*Ext1*$^{+/-}$ ("*Ext1*$^{+/-}$") brain sections are similar. **b** mCWD electrophoretic mobility and glycoprofile are also similar in *Ext1*$^{+/+}$ and *Ext1*$^{+/-}$ mice. **c** Representative example of PrP^{Sc} aggregate stability as measured by GdnHCl denaturation in mCWD-infected *Ext1*$^{+/+}$ and *Ext1*$^{+/-}$ mice. $[GdnHCl]_{1/2}$ values shown for mCWD in *Ext1*$^{+/+}$ and *Ext1*$^{+/-}$ brain (n=4 mice/strain; each run in triplicate).

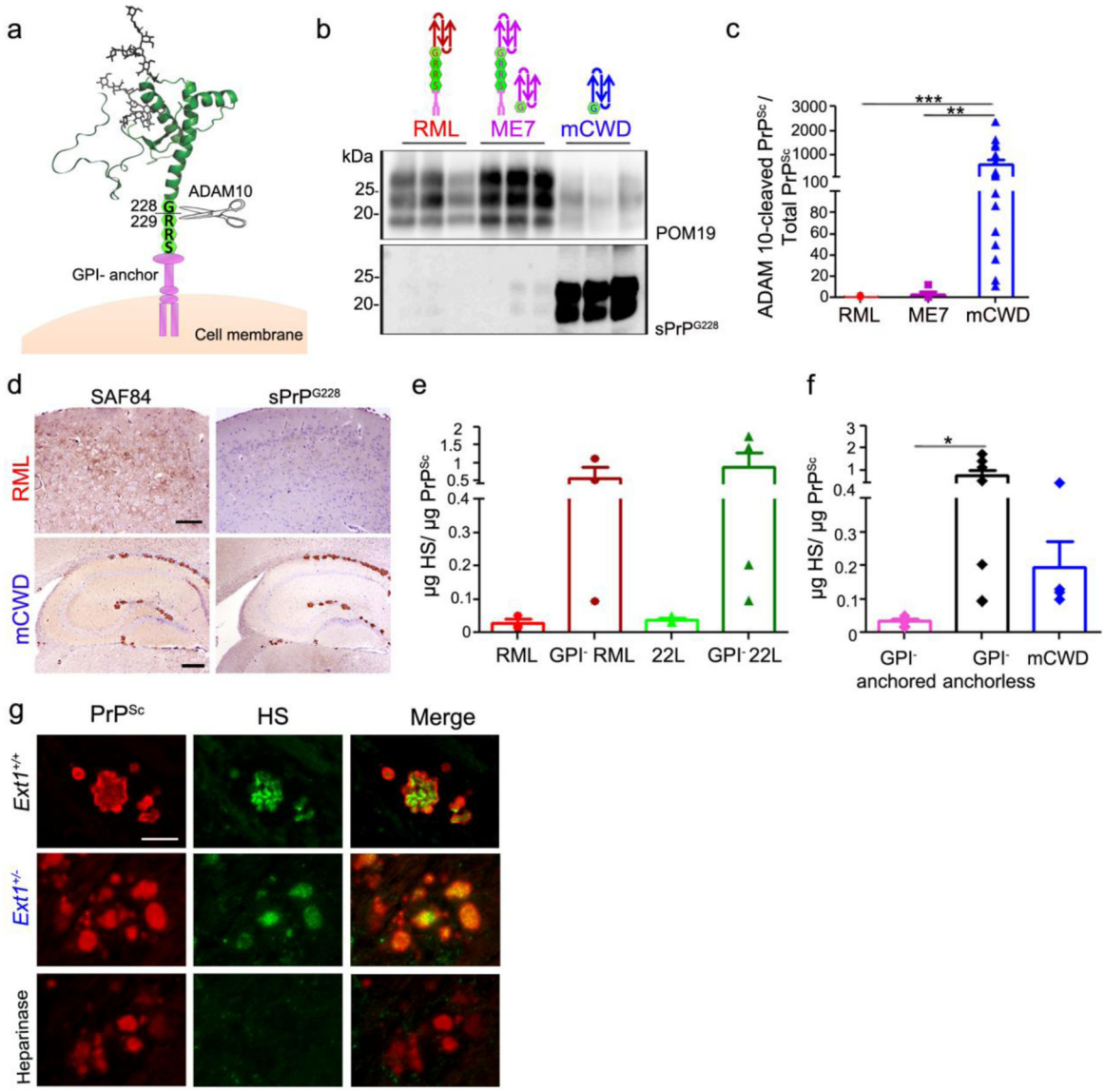

Fig. 4.

ADAM10-cleaved and full length GPI-anchorless prions bind HS. **a** Schematic representation of ADAM10 cleavage at mouse PrP residue 228 shows the release of shed PrP lacking the GPI-anchor and three C-terminal amino acid residues (RRS). **b** Immunoblots of brain homogenate from prion-infected *Ext1*$^{+/+}$ mice using POM19 antibody (PrP) and sPrP^{G228} antibody (ADAM10-cleaved PrP). **c** Ratios of ADAM10-cleaved PrP^{Sc} relative to total PrP^{Sc} reveal significantly higher levels of ADAM10-cleaved PrP in mCWD as compared to the RML and ME7 strains. **d** Brain immunolabelled for PrP with SAF84 (amino acids 163–169 of mouse PrP) and sPrP^{G228} antibodies reveals all mCWD plaques, but few diffuse RML aggregates, are labelled by sPrP^{G228}. **e** Quantification of HS bound to GPI-anchored and –anchorless RML and 22L prions by LC-MS, and **f** a grouped comparison of HS bound to GPI-anchored prions (RML and 22L) versus GPI-anchorless prions (GPI^{-} RML, GPI^{-} 22L) and ADAM10-cleaved mCWD shows that full length, GPI-

anchorless prions and ADAM10-cleaved prions (mCWD) bind more HS than their GPI-anchored counterparts. **g** Dual immunostaining of mCWD-infected brain sections for PrP and HS shows parenchymal prion plaques in the corpus callosum label strongly for HS. Pre-treating brain sections with heparinases abolished HS labelling of plaques. Scale bars = 200 μm and 500 μm for upper and lower panel (panel d) and 25 μm (panel g). *P< 0.05, **P< 0.01 and ***P< 0.001, Wilcoxon rank sum test (panel c) and one-way ANOVA with Tukey's post test (panel f).

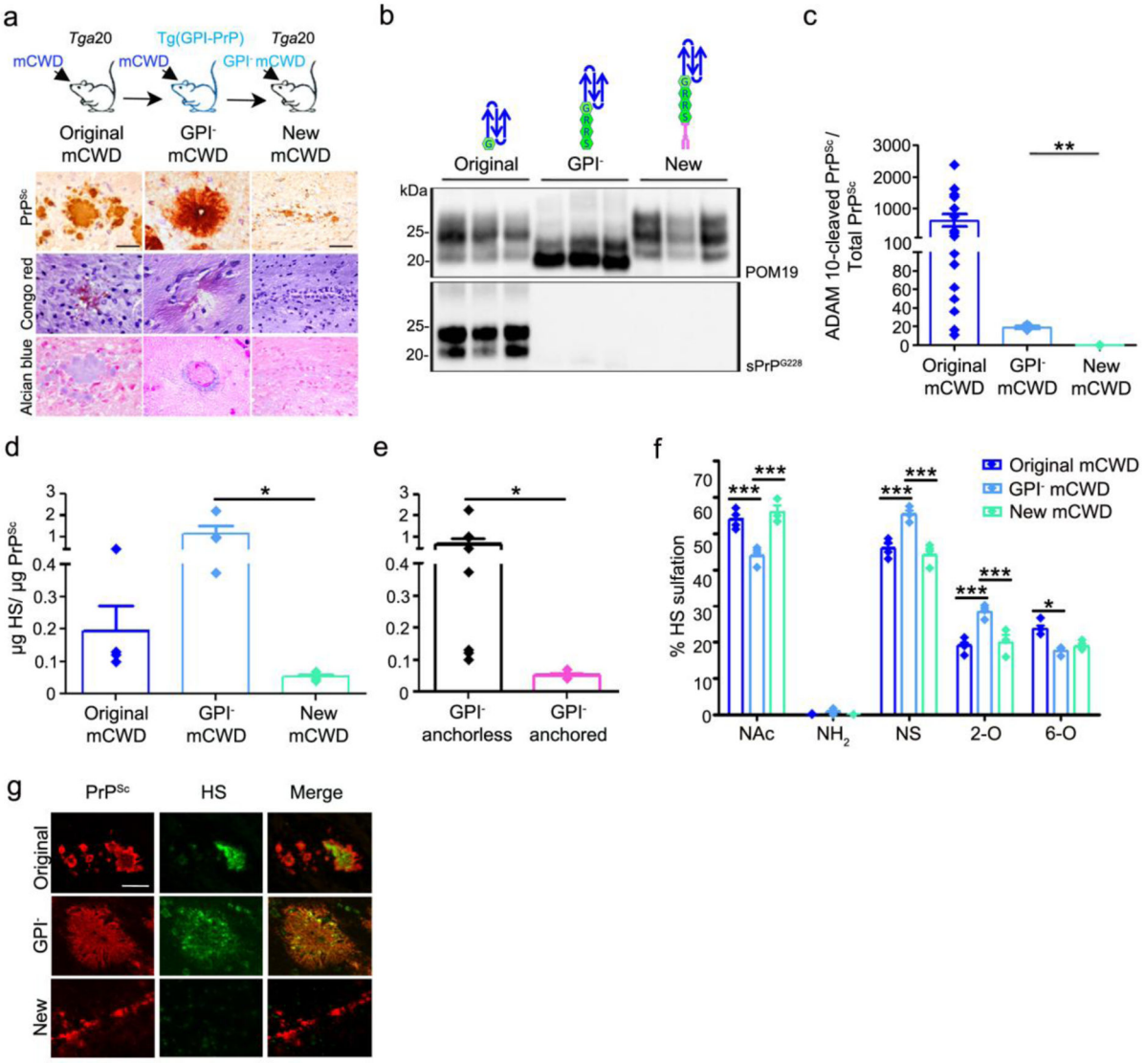

Fig. 5.

GPI-anchored mCWD prions do not form plaques and bind low levels of HS. **a** Schematic representation of mCWD inoculated into *tg*a20 and GPI-anchorless PrP^{C} expressing mice [tg(GPI-PrP)] with corresponding prion plaque morphology, Congo red, and Alcian blue staining of brain sections (corpus callosum). Note that the new mCWD prions do not bind Congo red or Alcian blue. **b** Western blots of PK-treated PrP labelled with anti-PrP POM19 (total PrP) or $sPrP^{G228}$ (ADAM10-cleaved PrP) antibodies reveal ADAM10-cleaved PrP in the original mCWD but not the GPI-anchorless mCWD or the new mCWD–infected brain. **c** Ratios of ADAM10-cleaved : total PrP^{Sc} are higher in the original mCWD than in the GPI-anchorless mCWD or in the new mCWD-infected brains (original mCWD results are also shown in Fig. 4c). **d** The new mCWD binds less HS than the original mCWD or GPI-anchorless mCWD (original mCWD results are also shown in Fig. 4f). **e** A grouped comparison shows HS bound to GPI-anchorless prions (mCWD and GPI^{-} mCWD, black bar) versus the new GPI-anchored mCWD (pink bar). **f** The HS bound to GPI-anchorless

mCWD is more sulfated than the HS associated with ADAM10-cleaved mCWD and the new GPI-anchored mCWD, as it contains less unsulfated N-acetylated (NAc) HS and higher level of N-sulfated (NS) and 2-O sulfated (2-O) HS. **g** HS does not co-localize to the new mCWD aggregates (bottom panel). Scale bars = 100 μm for original and GPI^{-} mCWD and 200 μm for new mCWD (panel a) and 25 μm (panel g). *P< 0.05, **P< 0.01 and ***P< 0.001, Wilcoxon rank sum test (panels c and e), one-way ANOVA with Tukey's post test (panel d), and two-way ANOVA with Bonferroni's post test (panel f).

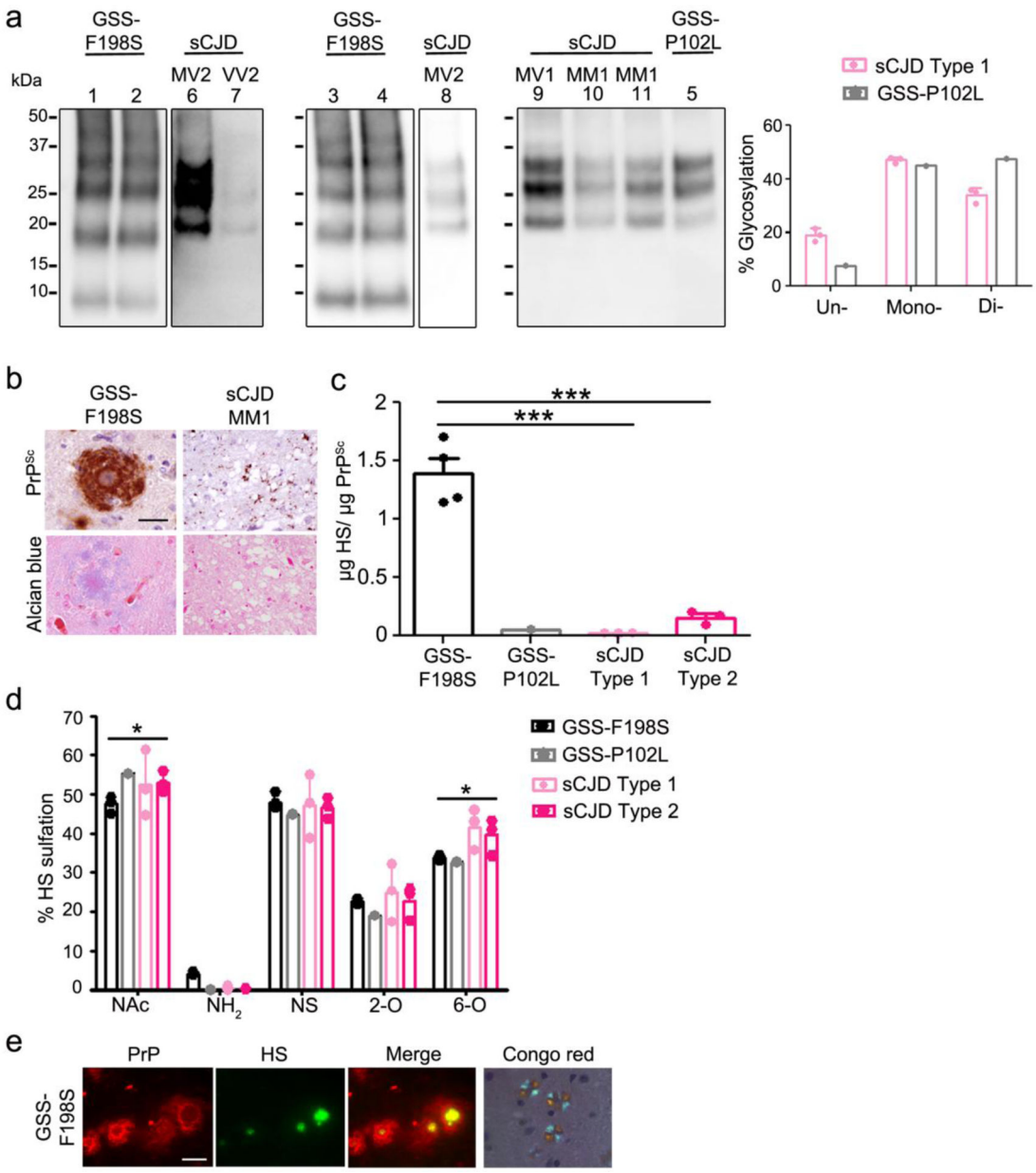

Fig. 6.

Abundant HS is associated with prion plaques in human brain. **a** Immunoblots of PK-digested PrP purified from GSS and sCJD brain samples show differences in electrophoretic mobility and glycoprofile. Note that PrP from the GSS-P102L brain shows a PK core size of 21 kD and a different glycoprofile than PrP from the sCJD MM1 and MV1 brain samples. **b** Fibrillar prion plaques from GSS-F198S patients immunolabelled for PrP. Plaques also bind Alcian blue. **c** Mass spectrometry of HS from purified prion preparations derived from the GSS and sCJD patient brain samples reveal significantly higher HS levels associated with the GSS-F198S purified prions. **d** The HS bound to GSS-F198S prions shows lower levels of N-acetylated (NAc) and 6-O (6-O) sulfated disaccharides than the HS bound to sCJD. **e** Cerebellar GSS-F198S plaques show intense HS immunolabelling, primarily in the plaque

core. Plaque cores in GSS-F198S affected brains are Congo red positive (shown is a representative example). Cerebellum (GSS-F198S) and thalamus (sCJD MM1) are shown in panel b. Scale bars = 50 μm (sCJD) and 100 μm GSS-F198S (panel b), 25 μm (dual IF, panel e) and 250 μm (Congo red, panel e). ***P< 0.001, One-way ANOVA with Tukey's post test (panels c). *P< 0.05, Two-way ANOVA with Bonferroni's post test (panel d).

Table 1.

Human cases used for heparan sulfate analysis.

Code	Age of onset	Disease duration (months)	Gender	*PRNP* genotype (mutation-129codon)	PrP^{Sc} subtype	Symptoms at disease onset	Family history of prion disease
1	49	120	M	F198S-129MV	GSS, 8 kDa	Cerebellar	Brother and niece
2	51	72	M	F198S-129VV	GSS, 8 kDa	Cerebellar	Brother and daughter
3	60	89	M	F198S-129MV	GSS, 8 kDa	Not reported	Father
4	67	63	M	F198S-129MV	GSS, 8 kDa	Not reported	Not reported
5	22	23	M	P102L-129MV	fCJD, Type 1	Seizures	Cousin
6	60	20	M	129MV	sCJD, Type intermediate+ 2	Visuospatial	Not reported
7	55	6	F	129VV	sCJD, Type 2	Apraxia	Not reported
8	55	24	F	129MV	sCJD, Type intermediate+ 2	Behavior	Not reported
9	69	6	F	129MV	sCJD, Type 1	Behavior/Memory	Not reported
10	60	1.5	M	129MM	sCJD, Type 1	Cognitive/Visual	Not reported
11	57	4	F	129MM	sCJD, Type 1	Motor	Not reported